SYNTHESIS OF NOVEL DIKETOPYRROLE AND SELENOPHENE CONTAINING NIR ABSORBING POLYMERS AND THEIR APPLICATION IN BULK-HETEROJUNCTION SOLAR CELLS

A THESIS SUBMITTED TO
THE GRADUATE SCHOOL OF NATURAL AND APPLIED SCIENCES
OF
MIDDLE EAST TECHNICAL UNIVERSITY

BY

GÜLCE ÖKLEM

IN PARTIAL FULFILLMENT OF THE REQUIREMENTS
FOR
THE DEGREE OF MASTER OF SCIENCE
IN
POLYMER SCIENCE AND TECHNOLOGY

SEPTEMBER 2017

Approval of the thesis:

SYNTHESIS OF NOVEL DIKETOPYRROLE AND SELENOPHENE CONTAINING NIR ABSORBING POLYMERS AND THEIR APPLICATION IN BULK-HETEROJUNCTION SOLAR CELLS

Submitted by **GÜLCE ÖKLEM** in partial fulfillment of the requirements for the degree **of Master of Science in Polymer science and Technology Department, Middle East Technical University** to,

Prof. Dr. Gülbin Dural Ünver Director,
Graduate School of **Natural and Applied Sciences** _____

Prof. Dr. Necati Özkan
Head of Department, **Polymer Science and Technology** _____

Assist. Prof. Dr. Görkem Günbaş
Supervisor, **Department of Chemistry, METU** _____

Examining Committee Members:

Prof. Dr. Ali Çirpan
Department of Chemistry, METU _____

Assist. Prof. Dr. Görkem Günbaş
Department of Chemistry, METU _____

Assist. Prof. Dr. Salih Özçubukçu
Department of Chemistry, METU _____

Assist. Prof. Dr. Erhan Bat
Department of Chemical Engineering, METU _____

Assist. Prof. Dr. Yunus Emre Türkmen
Department of Chemistry, Bilkent University _____

Date: 06.09.2017

I hereby declare that all the information in this document has been obtained and presented in accordance with academic rules and ethical conduct. I also declare that, as required by these rules and conduct, I have fully cited and referenced all material and results that are not original to this work.

Name, Last Name: Gülce Öklem

Signature:

ABSTRACT

SYNTHESIS OF NOVEL DIKETOPYRROLE AND SELENOPHENE CONTAINING NIR ABSORBING POLYMERS AND THEIR APPLICATION IN BULK-HETEROJUNCTION SOLAR CELLS

Öklem, Gülce
M.S., Department Polymer Science and Technology
Supervisor: Assist. Prof. Dr. Görkem Günbaş

September 2017, 78 pages

DPP-based conjugated polymers are recently used in organic light emitting diodes, electrochromic devices, organic field effect transistor and organic solar cell applications. Their advantageous properties, such as broad optical absorption in Near Infra Red (NIR) region, high charge carrier mobility and good film forming ability make them an excellent choice for generation of highly efficient solar cells. In this thesis, using donor-acceptor approach (D-A) we aimed to synthesize novel polymers with furan based DPP units as the acceptor and selenophene as the donor. Modulating the alkyl side chains on furan based DPP cores, we obtained three different monomers which coupled with selenophene via Stille Coupling. Oxidation and reduction behaviors of the synthesized polymers were studied with cyclic voltammetry. Optical absorption properties of the polymers were investigated. Bulk heterojunction solar cell application of one of these polymers, P3 was performed with polymer/PCBM (1:3) ratio and the devices were fabricated with the structure ITO/PEDOT:PSS/P3:$PCB_{71}M$/LiF/Al. Additionally, Inverted type bulk heterojunction solar cell application of P3 was also performed with device structure ITO/ZnO/P3:$PC_{71}BM$/MoO_x/Ag. While 3.00 % conversion efficiency was observed for the normal structure, a respectable 6.16 % efficiency was reached in the inverted structure with 3% diphenylether additive. This is one of the highest PCE reported for DPP based polymers.

Keywords: DPP, Near IR Region, Organic Solar Cells, Inverted solar cells

ÖZ

ÖZGÜN DİKETOPİROL VE SELENOFEN İÇEREN YAKIN KIZIL ÖTESİ BÖLGEDE SOĞURMA YAPABİLEN POLİMERLERİN SENTEZİ VE ORGANİK GÜNEŞ HÜCRELERİNDE UYGULANMASI

Öklem, Gülce
Yüksek Lisans, Polimer Bilim Ve Teknolojisi
Tez Yöneticisi: Yard. Doç. Dr. Görkem Günbaş

Eylül 2017, 78 sayfa

DPP-bazlı konjuge polimerler yakın geçmişte organik ışık yayan diyotlarda, elektrokromik cihazlarda, organik alan etkili transistörlerde ve organik güneş pillerinde kullanılmaktadır. Bu polimerlerin, Yakın Kızıl Ötesi (NIR) bölgede geniş optik absorpsiyon, yüksek yük taşıyıcı hareket kabiliyeti ve iyi film oluşturma gibi avantajlı özellikleri, onları verimli güneş pili çalışmaları için mükemmel bir seçim haline getirir. Bu çalışmada, donör-akseptör yaklaşımı (D-A) kullanarak, furan bazlı DPP birimleri akseptör ve selenofen verici olarak yeni polimerler sentezlemeyi amaçladık. Furan bazlı DPP iskeletleri üzerindeki alkil yan zincirlerini modüle ederek, Stille Coupling vasıtasıyla bağlanan üç farklı monomer elde ettik. Sentezlenen polimerlerin oksidasyon ve indirgenme davranışları dönüşümlü voltametri ile incelendi. Polimerlerin optik absorpsiyon özellikleri araştırılmıştır. Bu polimerlerden biri olan P3'ün bulk heteroeklem güneş pilleri uygulaması, polimer/PCBM (1:3) oranı ile gerçekleştirilmiştir ve cihaz çalışmaları ITO/PEDOT:PSS/P3:$PC_{71}BM$/LiF/Al yapısıyla uygulanmıştır. Ek olarak, P3'ün ters çevrilmiş hacimli heterojinasyonlu güneş pil uygulaması ITO/ZnO/P3:$PC_{71}BM$/MoO_x/Ag cihaz yapısı ile gerçekleştirildi. Normal yapı için %3.00 dönüşüm etkinliği gözlenirken, %3 difenileter katkılı ters yapıda önemli olarak %6.16 verim elde edildi. Bu, DPP esaslı polimerler için bildirilen en yüksek güç dönüşüm verimlerinden biridir

Anahtar Kelimeler: DPP, Yakın IR Bölgesi, Organik Güneş Pilleri, Ters Güneş Pilleri

ACKNOWLEDGEMENTS

I wish to express my most sincere gratitude and appreciaition to Assist. Prof. Dr. Görkem Günbaş for his guidance, understanding and patience. I thank him for his encouragement and support during my journey of science which was full of difficulties and surprises and thank him for always illuminating may way.

I would like to thank Prof. Dr. Levent Toppare for all his support during my graduate study, it was an unique opportunity to benefit from his knowledge and experience both in life and chemistry.

I am also thankful to Assist. Prof. Dr. Derya Baran and Xin Song from King Abdullah University of Science and Technology, for their collabration and their valuable contribution to this study.

My examining committee, Prof. Dr. Ali Çırpan, Assist. Prof. Dr. Salih Özçubukçu, Assist. Prof. Dr. Erhan Bat and Assist. Prof. Dr. Yunus Emre Türkmen for accepting to evaluate my thesis and their valuable suggestions.

I would like to thank Prof.Dr. Teoman Tinçer for all his support to encourage me during my master study.

I would like to thank Gönül Hızalan with all my heart, not only for solar cell applications but also for her support and frienship and giving a shoulder to cry on.

I would like to thank Şerife Özdemir Hacığolu and Assoc. Prof. Dr. Yasemin Arslan Udum for electro chemical studies.

I would like to thank Seza Göker and Şevkican Cevher for sharing their polymerization experiences and their valuable suggestions and answering all my questions everytime I needed.

Also I would like to thank all Toppare, Çırpan and Özçubukçu group memebers, for always

well coming me to their laboratories, helping me whenever I needed and sharing everything they had.

I woul like to thank Gizem Atakan, it was so nice to have someone like you as a friend and as a boss, who deals with problems gently and never lose the smile on her face, thank you for your all support and advices both in laboratory and life .

Many special thanks to Aliekber Karabağ, our talented, handy man, helps everytime a short girl needs and also I am grateful to your generous donation of 9-(Bromomethyl)nonadecane.

I am grateful to have chance to know Osman Karaman, with his sweet surprises for late night column victims, the times when you try to cheer me up, were always worth for rebemmbering, thank you.

I would thank to Esra Bağ for the times she shared with me and my never ending columns, and thank you making it fun with your heart to heart talks.

My sincere thanks to all EGGs, sharing D-150 all together; with exploding experiments, never ending columns, with all the butyls in the fridge, with coffee breaks, with all the good and bad times, thank you for all of you, all my lab memories are special for me.

Şevkican Cevher, for his patience while synthesis of 9-(Bromomethyl)nonadecane, Gencay Çelik for healthy/unhealthy snacks exchange, Nima Sohrabnia and Pelin Yuşan for their true friendship, thank you again.

Halil Memiş, thank you for your help, commnets, suggestions I always feel lucky to meet with you.

Betül Eymür thank you for your special help with my weird NMR samples and sorry fort he pink dots on the wall.

Thank you my Izmir girls, Ecem Arslanay, Serra Rodoplu, Pınar Dinçer and Didem Sone, sharing the dusty roads of Ankara all together with the best memories.

There are also no enough words to express my gratitude to Didem Sone. I will always feel lucky to have some one in life as a friend. Without your frienship and your support those years would never be easy.

Finally to my dear mother and dear father, to all your patience and support that you provided me for years, I am greatful. During my long education journey, thank you being always beside me.

To all the women in science,

TABLE OF CONTENTS

LIST OF TABLES

LIST OF FIGURES

FIGURES

LIST OF ABBREVIATIONS

c-Si	Mono-crystalline
mC-Si	Multi crystalline
PERC	Passivated Emitter and Rear Cell
PESC	Passivated Emitter Solar Cell
PERL	*Passivated Emitter Rear Locally*
a-Si	Amorphous silicon
TCO	Transparent Conducting Oxide
CBD	Chemical Bath Deposition
CSS	Closed Space Sublimation
PV	Photovoltaic
BHJ	Bulk Heterojunction
IR	Infra-Red
OPV	Organic Photovoltaic
PEDOT	Polyethylenedioxythiophene
DPP	Diketopyrrolo-pyrrole
DDQ	2,3-Dichloro-5,6-dicyano-1,4-benzoquinone
ITO	Indium Tin Oxide
PCE	Power Conversion Efficiency
LUMO	Lowest Unoccupied Molecular Orbital
HOMO	Highest Occupied Molecular Orbital
E_g	Band Gap
QE	Quantum Efficiency
J_{sc}	Short Current Density
EQE	External Quantum Efficiency
FF	Fill Factor
AFM	Atomic Force Microscopy
TEM	Transmission Electron Microscopy

PSS	Polystyrene Sulfonate
DPE	Diphenyl Ether
ACN	Acetonitrile
CV	Cyclic Voltammetry

CHAPTER I

INTRODUCTION

1.1 Brief History

Today solar energy is perceived as a late twentieth century phenomenon; however, humankind had discovered the energy of the sun 6000 years ago. Many prehistoric tribes proclaim the sun as a god, realizing the sun is the source of every natural phenomenon. Stone Age Chinese built their homes such a way to provide utmost benefit to the sun. The Great Pyramid in Egypt which is one of the most perfect architectural achievement of mankind, was built to be a staircase to the sun [1]. Sun is the resource of life on Earth, presenting the different forms of energy; biofuel, thermal and electrical. Statistics presume that growing electrical energy demand will be doubled by the year 2030. The amount of energy of which the Sun delivers to Earth is 1.2×10^5 terawatt and daily energy consumed on Earth is 13 TW [2].

The story of solar cells began in 1839, with discovery of photovoltaic effect by Edmond Becquerel, immersing the two different brass plates into a liquid, resulted generating a continuous current when exposed to sunlight. In the late 1870s, Willoughby Smith, W. G. Adams and R. E. Day discovered the photovoltaic effect in selenium, followed by the first solar cell, transparent gold film coated selenium on a metal, created by C.E. Fritts, 1885. Developments in solar cells studies accelerated after the discovery of quantum mechanics. In 1954 at Bell Laboratories, by replacing the selenium with silicon crystal, scientist invented the first practical solar cell with 6 % efficiency. The most important reason for the increased interest in solar cell research was the space explorations in late 1950s and the oil crisis in 1970s. As the need for solar cells increased, new varieties have begun to be developed for different application areas [1-3]. With ever increasing material choices and advancing device structures, organic solar cells keep improving their power conversion efficiencies since they first discovered.

1.2 Types of Solar Cells

1.2.1 Mono-Crystaline and Multi-crystaline Silicon Solar Cells

By being the first discovered solar cell in 1950s, and as well as the improvements in microelectronics, crystalline silicon solar cells have grown much faster than the other photovoltaic technologies. Highest efficiency recorded 25.6% in 2016, pushing the theoretical limits which were calculated as 33.5% [3]. Silicon is an advantageous material for solar cell applications, having low energy band gap of 1.12 eV of silicon makes it compatible with solar spectrum, providing the long term outdoor stability when compared with other materials. Crystalline silicon photovoltaics also known as first generation solar cells, include both mono-crystalline (c-Si) and multi crystalline (mc-Si) types of silicon [3].

1.2.1.1 Mono-Crystalline Silicon Solar Cells

Mono-crystalline silicon solar cells are made from highly pure silicon wafers containing almost no defect or metal impurity. In these cells, the silicon has a single continuous crystal lattice structure [4]. Manufacturing highly pure silicon is a complicated and expensive process which leads to relatively high costs. However, modules made from mono-crystalline silicon solar cells are widely used in both space and commercial applications. The recent efficiency of multi-crystalline silicon solar cell was reported as 20.4%. The PESC, PERC and PERL applications, all are advances in surface passivation, reduce recombination of charge carriers on the surface and improved the efficiency [3].

1.2.1.2 Multi-Crystalline Silicon Solar Cells

Multi crystalline silicon solar cells, known as polycrystalline cells are produced from multiple grains of monocrystalline silicon. Multicrystalline cells are cheaper than monocrystalline ones because of the simpler method in production. Compared with monocrystalline silicon solar cells, multi crystalline silicon solar cells have less efficiency due to more impure nature [4].

1.2.1 Amorphous Silicon Solar Cells

Amorphous silicon (a-Si) contains 10% hydrogen and named as glassy alloy of silicon and hydrogen. Amorphous silicon solar cells differ from mono- and multicrystalline solar cells in a way that the silicon atoms are arranged in a thin homogenous layer. Thin film photovoltaic technology emerged with amorphous silicon solar cells. When compared with crystalline solar cells, amorphous silicon cells have a better light absorption and this is the reason that they can be used in the production of thinner cells [4]. Since early 1980s amorphous silicon solar cells have been used in calculators and digital watches, in mid 1980s solar module applications of amorphous silicon has been accelerated [5].

Amorphous silicon solar cells have lower efficiencies than crystalline solar cells, around 6-7% [6]. However, they are easier and cheaper in production therefore there are many application areas. In order to improve efficiency, various designs of hybrid modules increased, a-Si is combined with the layers of multicrystalline silicon (9-10% efficiencies). Recent studies predicted that 13% efficiency for amorphous silicon technology can be achievable by embedding the metallic nanoparticles (MNPs) inside the structure [6].

1.2.2 Cadmium Telluride Solar Cells

Thin film cadmium telluride (CdTe) is one of the practical material among the photovoltaic technology due to its ideal band gap 1.5 eV, high absorption property and the outstanding chemical stability [4]. Theoretical efficiency for CdTe solar cells were calculated around 28% - 30%. The recent studies seem to be close to the foreseen efficiency values, recording 22.1% by First Solar Inc.US [7].

In the typical device architecture of CdTe/CdS solar cells, there are 4 layers;

1. TCO-transparent conducting oxide
2. CdS film as a window layer
3. CdTe film as an absorber layer
4. The back contact which on top of the CdTe layer [8].

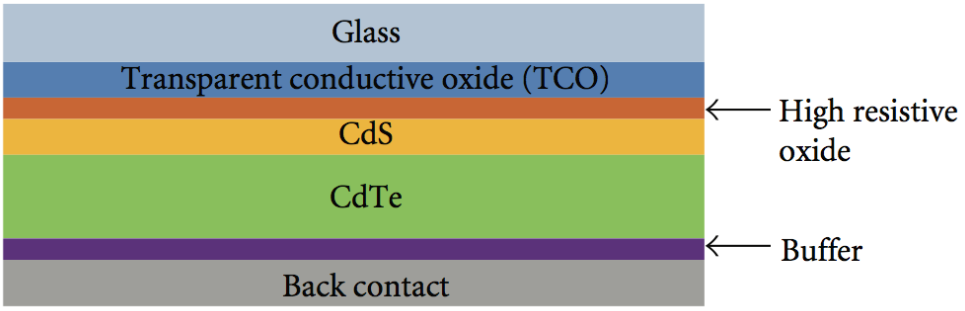

Figure 1.1: Structure of standard CdS/CdTe thin- film solar cells [8]

SnO_2, In_2O_3, ZnO, or Zn_2SnO_4 are the example materials for TCO films with high transparency ranges between 80%-90%. The next layer CdS; can be prepared by using different methods including chemical bath deposition (CBD) and closed space sublimation (CSS). CBD method is more preferable due to its higher efficiency record solar cell provided by compact film forming property. Another important step for high efficiency in CdTe solar cells is Cl_2 treatment for both CdTe and CdS layers. This step provides better interface [9].

1.2.3 Perovskite Solar Cells

Perovskite term defines the specific crystal structure with formula ABX_3 as calcium titanium oxide ($CaTiO_3$). X is oxygen or halogen, A is larger metal cation occupies the cubo-octahedral site shared with twelve X anions and B is smaller metal cation is coordinated in octahedral sites. The materials with this crystal structure exhibit different properties; ferroelectricity or superconductivity [10]. First studies on perovskite solar cell applied by Miyasaka et al in 2009, power conversion efficiency was found 3.8% for $CH_3NH_3PbI_3$ as an organic-inorganic sensitizer. In early application method of perovskite solar cells, the pigment was deposited in a single step onto metal oxide film using mixture of PbX_2 and CH_3NH_3X. Burschka et al., 2013 investigated a new method which started with applying PbI_2 first onto nanoporous titanium dioxide film, followed by transformation into perovskite in the

presence of CH_3NH_3I solution [11]. This technique resulted better morphology control and higher power conversion efficiency, 15%, was achieved [11].

1.2.4 Organic Solar Cells

Organic solar cells are considered as being one of the most promising alternative among the photovoltaic technologies thanks to their advantages. Organic solar cells offer advantages like low cost production, flexibility, thinnes and light weight devices [12-15]. As a result of the improvements in polymer synthesis, conjugated polymers have taken their place among the most important semiconducting materials. Photovoltaic properties of conjugated polymers like polyacetylene, derivatives of polythiophene and poly(phenylenevinylenes) gained attention when the mobile photoinduced charge transfer concept was understood [16-18].

The ultrafast, metastable and reversible transfer between conjugated polymer and fullerene is known as photoinduced electron transfer. The transfer of phoexcited electron from the conjugated polymer to the acceptor unit (mostly fullerene) occurs [14-18]. The resulted cation radical species named as positive polaron on the conjugated backbone are highly delocalized and stable as indicated in electrochemical or chemical oxidative doping studies [16]. Figure 1.2 shows the schematic representation of photoinduced electron transfer between conjugated polymer and fullerene .

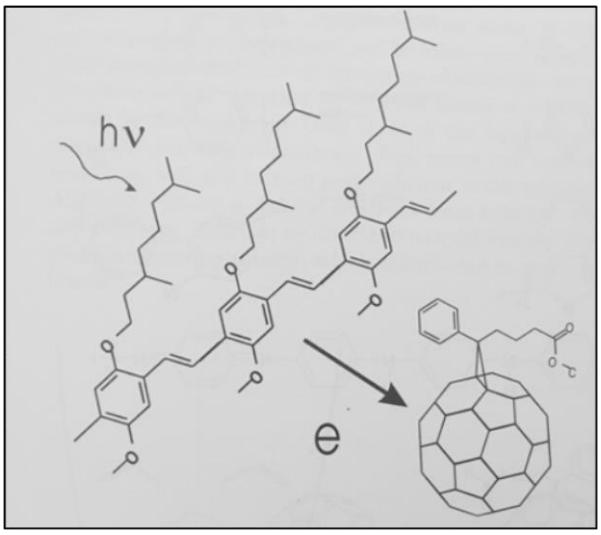

Figure 1.2: Photoinduced electron transfer between conjugated polymer and fullerene [13]

In working principle of organic solar cells photovoltaic active layer is sandwiched between the two electrodes. Photoexcitation of the donor material by the absorption of light energy generate excitons. This electron-hole pairs called excitons bounded by columbic forces diffuses in the active layer, composed of donor and acceptor. In donor-acceptor interface exciton dissociation occurs via electron transfer. Photocurrent and photogeneration occurs when the free charge carriers reach and collected in corresponding electrodes [16,18]. The limitations of the process are the short lifetimes of excitons (1ns) and their diffusion lengths (10-20 nm) in active layer [16-19]. This is the one of the main reasons that affects device performance due to loss of absorbed photons and quantum efficiency. Thus once the excitons are formed they have to diffuse into interface to convert to charge carriers before deactivating to ground state. The relation between exciton diffusion length and diffusion coefficient is expressed by the formula:

$$L_D = (D\,\tau)^{1/2}$$

L_D *:* Exciton diffusion length

D *:* Diffusion coefficient

τ: Exciton lifetime

Due to short lifetimes of excitons and limited diffusion lengths, only a limited part of excitons can diffuse into interface [17-19].

Bulk heterojunction concept (instead of layered structures of donor and acceptors) was introduced as a solution of limited exciton diffusion length which offers to form a bicontinues interpenetrating network for efficient exciton diffusion [14,19]. In order to increase excitons harvested in interface BHJ concept provides more smaller domain sizes than the exciton diffusion length. However, there is a contradiction between small domain sizes and charge collection because too small domain sizes contribute to charge recombination. Therefore exciton diffusion length and the morphology of the active layerhas asignificant effect on the device performance [20]. Bulk heterojunction concept is superior to bi-layer organic cells since the diffusion length of excitons are low. Hence charge separation can only happen on the interface where two layers are in contact with each other.As can be seen from the figure 1.3, active layers are coated on one top of another in bilayer structure which results in discontinued domains and thicker interface that excitons cannot diffuse efficiently [19].

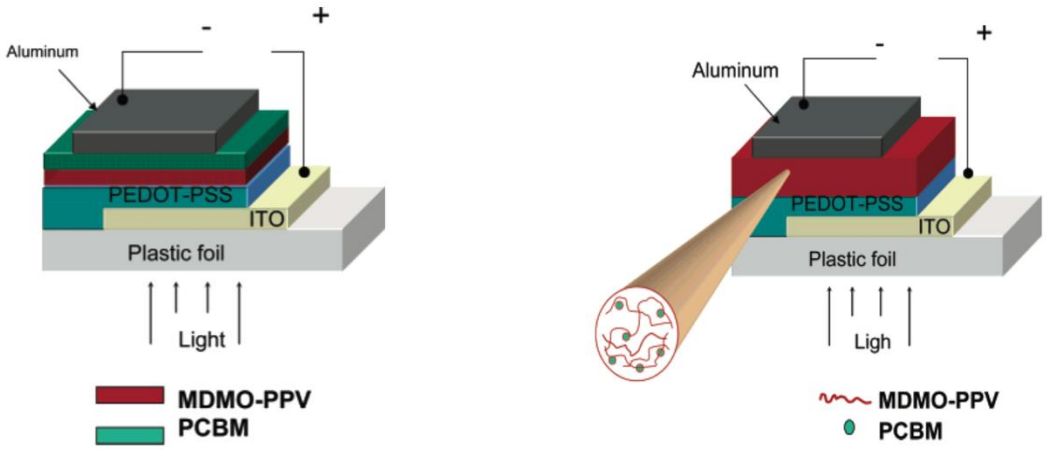

Figure 1.3: (a) Bilayer structure of an organic solar cell (b) Bulk heterojunction structure of oan organic solar cell [19]

In order to develop high performance in organic solar cells, one of the key parameter is the tuning the HOMO level of p-type polymer and the LUMO level of n-type PCBM derivative.

Band gap (E_g) is defined as total characteristic effects which arise from the nature of the polymer.

$E_g = E^{\delta r} + E^{\theta} + E^{res.} + E^{sub.} + E^{int}$

$E^{\delta r}$: bond length alternation along the chain

E^{θ}: mean deviation from planarity

$E^{res.}$: aromatic resonance energy of the ring

$E^{sub.}$: inductive or mesomeric electronic effects of substitutients

$E^{int.}$: inter-chain or intermolecular coupling in the solid state.

Low band gap polymers are known having a band gap smaller than 1.6 eV and this property enables them to make absorption in wider range including near IR region and result in harvesting more light to convert electricity. Using donor-acceptor (D-A) approach developed by Yamamoto *et al*., it is possible to create new altered HOMO and LUMO levels [21]. When two units with donor and acceptor properties are polymerized, HOMO of the donor and HOMO of the acceptor molecule create new HOMO level, while LUMOs of the donor and acceptor units interact to form a new LUMO level resulting a narrower optical band gap, depicted in Figure 1.4 [20].

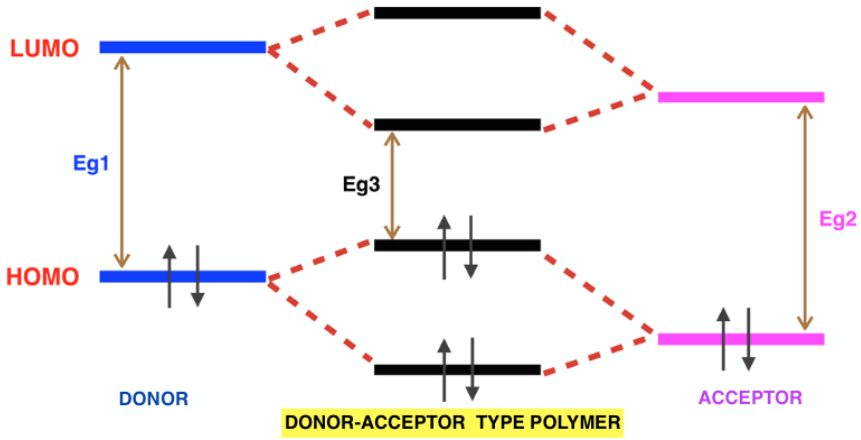

Figure 1.4: Simplified mechanism of bandgap lowering by donor−acceptor interaction [20].

1.2.4 Inverted Organic Solar Cells

Increasing interest in inverted solar cells in recent years is due to their device structure that exhibit better performance in harvesting more photons compared with normal device structures [22].

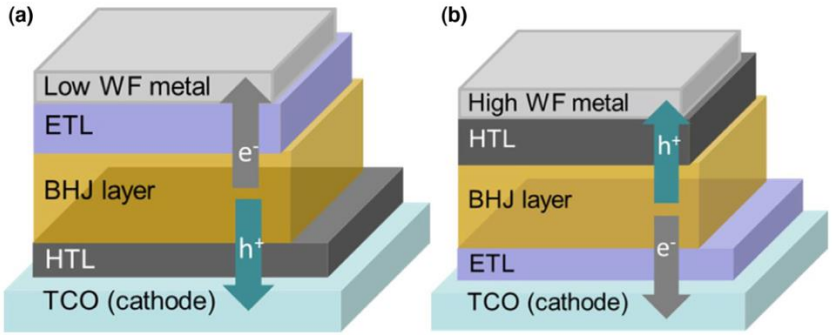

Figure 1.5: General device structures for (a) Conventional organic solar cell and (b) Inverted organic solar cells [22]

The main differences arise from the substitution of the low work function metal with high work function metal in order to overcome stability limitations [23]. In general, device architecture of a typical organic bulk heterojunction solar cell is ITO/PEDOT:PSS/photoactive layer/LWF metal. LWF metals such as Li, Ca and Al, can be easily oxidized [23]. Diffusion of the oxygen into photoactive layer through pinholes and grain boundaris through to cathode causes deterotion of the structure of active layer [23]. However, inverted device structure offers an improvement about air stability of the devices by using ITO as a cathode and a high work function (HWF) metal as an anode such as Ag, Au and Cu [23,24]. Furthermore, inverted-structure solar cells differ from the conventional solar cells by having the opposite sequence of hole blocking layer between the transparent electrode and electron blocking layer on the top contact with a high work function metal silver or gold having the air stability [22, 24]. The first inverted organic solar cell was reported by Shirakawa et al. applying ZnO hole- blocking layer and a gold layer as top electrode [25]. In 2016 Cho et al.,

reported 10.08% power conversion efficiency by introducing a novel method using gradiently doped ZnO ripple structures and alkali metal carbonates with bilayer deposition [26].

1.3 DPP Polymers For Organic Solar Cells

Since the first discovery of the DPPs, they are used in various industrial applications, including paints, varnishes and printing. Their bright colors and high stability make them excellent choice for various applications. More recent studies reveal that DPP based materials can be successfully utilized in semiconductor technology such as OFETs, solar cells and OLEDs. DPP–based conjugated polymers are the promising materials which meet most of the requirements of an efficient organic solar cells; broad optical absorption, good film forming properties, and better morphology lead to improved fill factor (FF) and high short-circuit current (J_{sc}) [27]. Characteristics of self-assembly towards to more ordered domains make DPP-based molecules can easily be modified by both alkyl side chains or other functional groups. The structure property of the polymer has an immense effect on solar cell device performance by effecting the light harvesting ability, energy levels, solubility, charge carrier mobility and film forming characteristics of the active layer. The length, branching, position and symmetry of the alkyl side chain have a direct effect on molecular packing and crystallinity which adjust the film morphology [27]. Another correlation has been confirmed between the end groups and optoelectronic properties, charge generation, transportation and collection process in an organic cell device [27]. Hence having easily modifiable positions make DPP a great candidate for organic electronic applications.

First applications of DPP- based small molecules and polymers in organic solar cells were achieved by Janssen and Nguyen separately but in the same time, in 2008 [28, 29]. Nguyen and co-workers utilized the DPP in a small chain oligothiophene derivative. The aim was to generate solution processable materials that exhibits stronger absorption in longer wavelengths. Thus, 3,6-diaryl-2,5-dihydro-pyrrolo[3,4-c]pyrrole-1,4-dione was used which served as a highly absorbing chromophore. This

design provided optical absorption at 720 nm in solution and 820 nm in the film. Thus, 2.3% power conversion efficiency with 70:30 donor/ acceptor ratio using [6,6]-phenyl C_{61} butyric acid methyl ester (PCBM) as an acceptor molecule in bulk heterojunction solar cell application. [27,28].

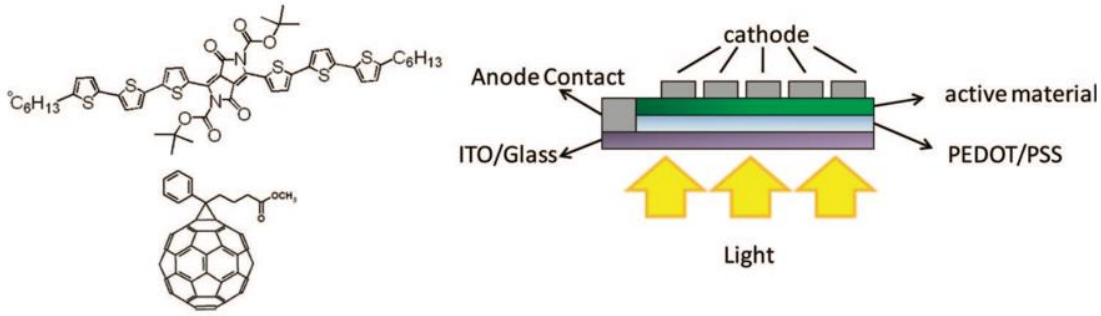

Figure 1.6: DPP and PCBM molecules [28]

Janssen group designed polymers consisted of electron rich quaterthiophene(BBT) moiety and electron poor diketo pyrrolo-pyrrole (DPP) unit towards achieving lower optical band gap (low as 1.4 eV). Poly[3,6-bis-(4' -dodecyl-[2,2']bithiophenyl-5-yl)-2,5-bis-(2-ethyl-hexyl)-2,5-dihydropyrrolo[3,4-]pyrrole-1,4-dione] (pBBTDPP2) (DPI=3.35), blended with [60]PCBM and [70]PCBM in orthodichlorobenzene solution provided 3.2% and 4.0% power conversion efficiencies respectively [29]. The significant difference arised in power conversion efficiencies due to the relatively higher absorption coefficient of [70]PCBM molecule in visible region [30].

1.4 Synthetic Methods For DPP

First discovery of DPP was a total coincidence rather than a consciously desired synthesis. In 1974 Farnum and co-workers obtined DPP as a byproduct of *beta*-lactam synthesis under Reformatsky conditions. Although not having the desired product, DPP was obtained as one of the low yielded (5-20%) by products. The characteristics of the molecule; bright red color and low solubility were the evidence that the product was an organic pigment [30, 31]. Chemists from Geigy AG (currently part of BASF)

focused on more efficient synthetic methods for DPP. Researchers found out the mechanism explained by Farnum et al., was incorrect. It was concluded that aminoester or zinc salt cannot dimerize to yield DPP.

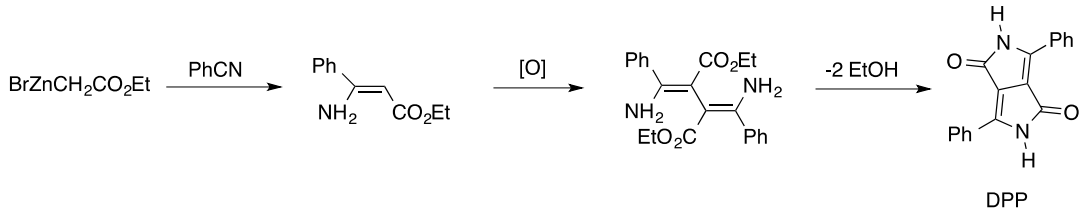

Figure 1.7: Postulated mechanism of DPP under Reformatsky conditions [30].

The revised mechanism of DPP synthesis under Reformatsky conditions is as follows figure 1.8:

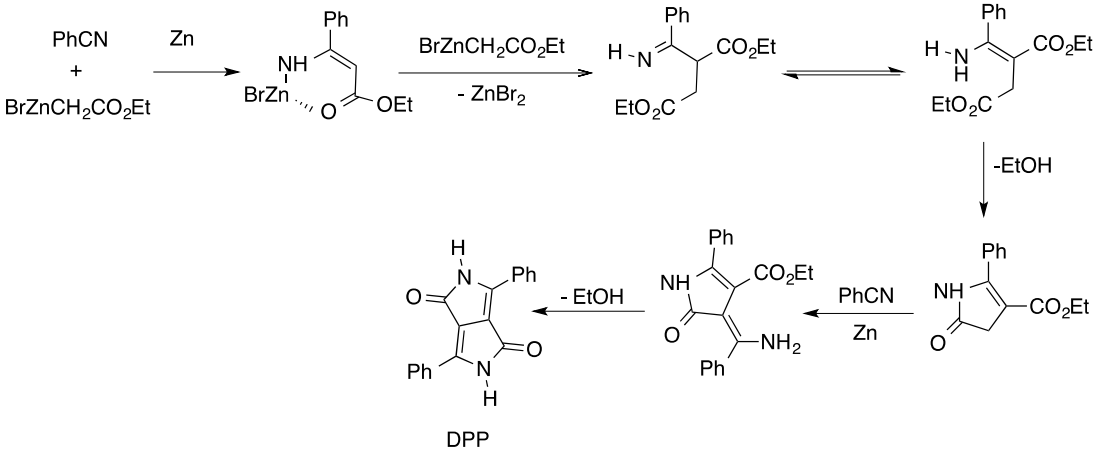

Figure 1.8: Revised mechanism of DPP formation by the Reformatsky route [30].

Later the synthetically improved method provided 30% yield for ethyl acetate and 60 % yield for nitrile used was still not enough for industrial production. Although the synthesis of DPP under Reformatsky conditions was improved by Shaabani and co-workers in 2005, succinic acid method has been frequently used since it was first introduced by Iqbal and co-workers 1988 [30].

Thus, compared with alternative methods, succinic ester and aromatic nitrile synthesis

provides less number of reaction step and requires more readily available starting materials which results in this method being the more practical synthetic option.

In this method, DPP product is obtained by direct cyclization reaction of aromatic nitrile and succinic ester. Branched alcohols and their sodium salt are used as the solvent and the strong base respectively.

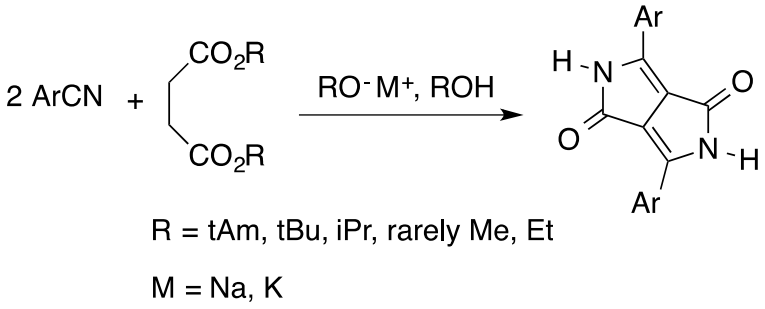

Figure 1.9: Succinic method of DPP synthesis [30].

Several other methods have been developed for DPP synthesis in recent years, including microwave heating or using DDQ as an oxidant. These methods, however resulted with variable slightly different yields and were not developed furthermore. Although the succinic acid method has been the most generally accepted method for synthesis of DPP molecules, it is only valid for symmetric molecules, not useful for asymmetric DPP derivatives. In order to have unsymmetrical product, starting with mixed aromatic nitriles can be considered, however due to low solubility of DPP molecules, it is not possible to separate the low yielded asymmetrical and symmetrical products from eachother [30]. One of the common method for unsymetrical DPP synthesis was proposed by the chemists at Ciba-Geigy. Under basic conditions it is possible to synthesize DPP by the reaction of a nitrile and an aminoester or a lactam [30].

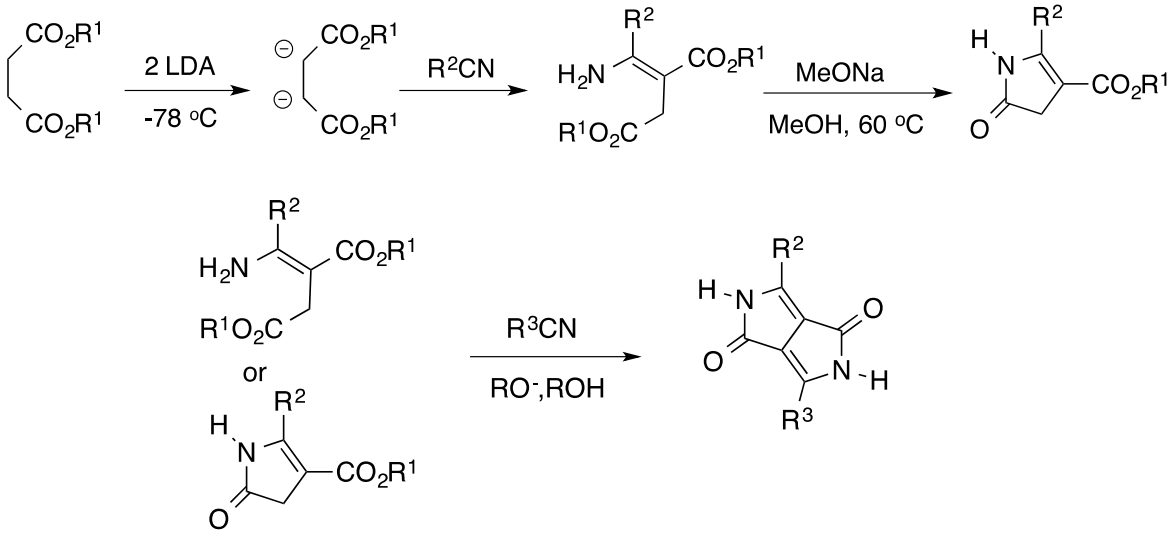

Figure 1.10: DPP synthesis from lactam and aminoester [30].

Both symetrical and unsymetrical DPP derivatives can be synthesized by this reaction route. Electron poor, unhindered nitriles provide the higher yields as in the succinic method [28-30]. When compared with lactam and aminoester precusors are compared, lactam is preferred in synthesis of asymetrical DPP because it's relatively more stability over the aminoesters [28].

1.5 Additives in Bulk Heterojunction Organic Solar Cells

In our study, we aim to investigate the additive effect on morphology and the resulted effect on efficiency. Various techniques have been applied such as thermal annealing, solvent vapor annealing and using different type of additives including small molecules, polymers, inorganic crystals and high boiling solvents [31,32]. Among these methods, morphological control by additives showed DPP based polymers can be significantly improved with the presence of the certain amount of additives resulting in higher efficiencies in solar cell applications [33, 34]. Recent studies demonstrate the more favorable effect of additives on morphology by altering the donor acceptor phases and domain sizes also enhancing crystallinity [32-37]. By introducing certain amount of additives, it is possible to decrease domain sizes and

prevent agglomeration in active layer. Therefore, providing increased improved area with an ideal morphology for charge generation and collection [37]. In 2008, Lee et al., specified the general characteristics of the additives for bulk heterojunction solar cells as (i) selective solubility to the one component and (ii) higher boiling point than the host solvent [38,39]. The study of Liao et al., represented the frequently used solvent additives in Figure 1.11 [32].

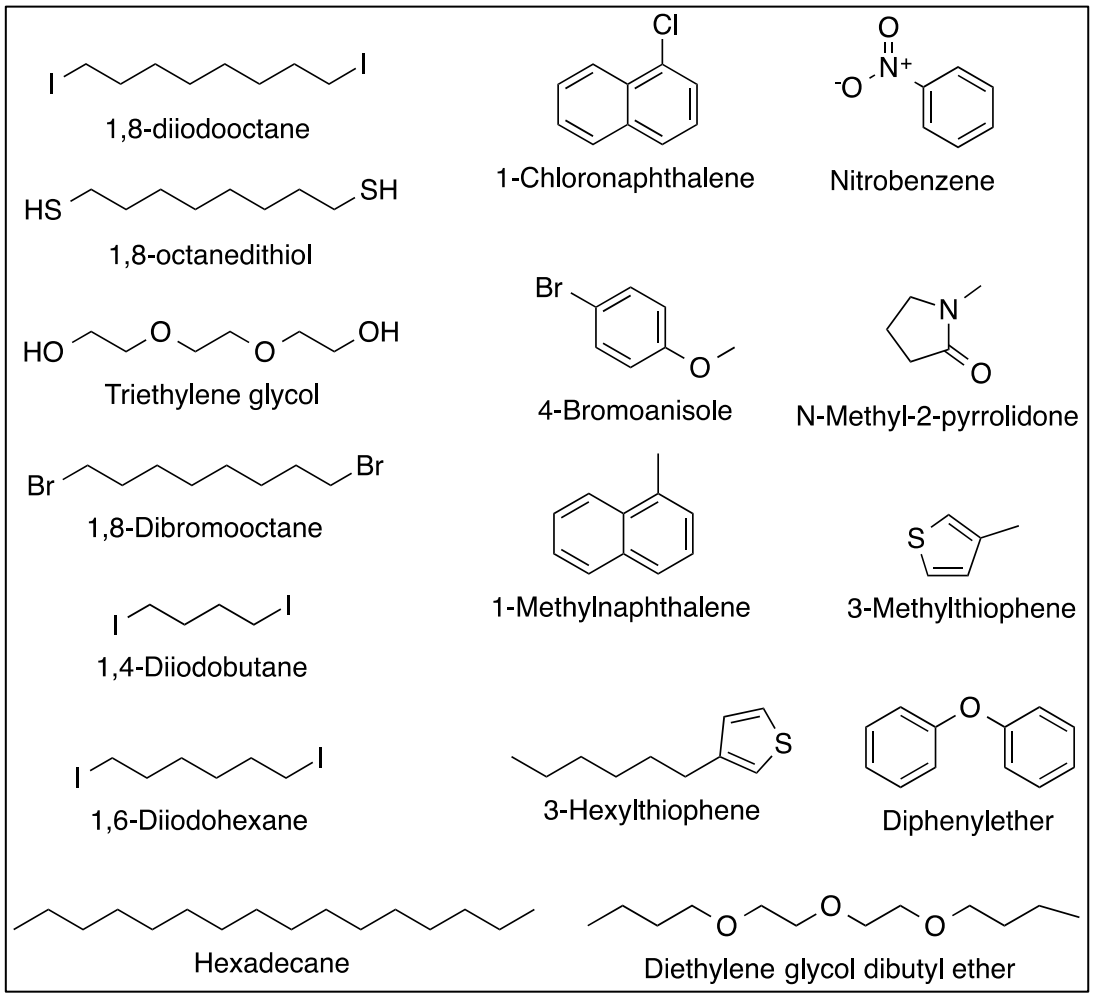

Figure 1.11: Examples of solvent additives for BHJ morphological control [32]

Frechet group in 2011 achieved 6.5% power conversion efficiency in DPP based organic solar cell application with presence of 1-chloronaphthalene (CN) additive

while the recent study of Heeger group reported DPP based organic solar cell reached efficiency 9.4% with presence of diphenylether additive [33,40].

1.6 Aim of the Study

The aim of this study is to synthesize novel DPP and selenophene containing polymers which have absorption ability both in visible and near IR regions and providing 5% power conversion efficiency. We were inspired by the fact that since DPP-based donor polymers exhibit broad optical absorption and high motilities for charge carriers they can give remarkable power conversion efficiencies as high as 9.4% [40]. We started our synthesis with furan based DPP molecules which is known for providing higher solubility than its thiophene analogue. Using the benefits of donor-acceptor approach we chose selenophene as donor for DPP acceptor moiety. Studieds in literature showed that selenophene containing DPP polymers exhibited high charge carrier mobilities [36,41]. Morever, selenophene unit has positive impact on solubility, film forming ability and morphology of the polymer [42]. Modifying the alkyl side chains in our DPP cores we synthesized three different polymers and observed that all exhibits different solubility, film forming and morphological properties. Polymerization of the furan based DPP unit and selenophene by Stille coupling reaction yielded polymers with a wide absorption spectra both in visible and NIR regions as expected. For achieving 5% power conversion efficiency we followed the study of Frechet et al, and used additives choloronapthalene and diphenyl ether both in conventional bulk heterojunction application and inverted solar cell applications. We finalized our study by developing 6.16% efficiency solar cells in collaboration with Baran Group at KAUST by using our novel structured **P3** as the active layer.

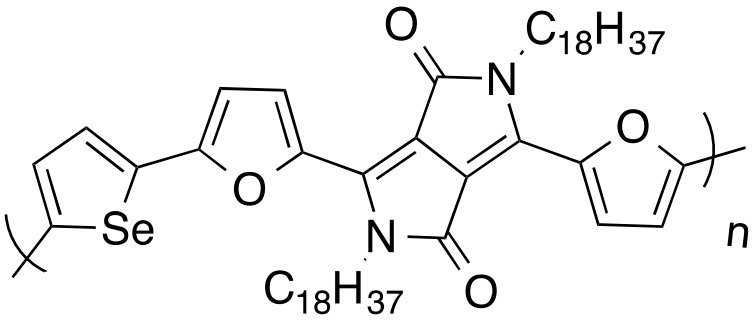

Figure 1.12: Structure of **P3**

CHAPTER II

EXPERIMENTAL

2.1 Materials

All chemicals were purchased from Sigma Aldrich, TCI and Carlo Erba. Dry solvents THF and DMF were obtained from MBBraun solvent dryer system which was available in the laboratory. For column chromatography, Merck Silica Gel 60 mesh was used as a stationary phase. All reactions were monitored with TLC and conducted under argon atmosphere unless otherwise was mentioned. Experimental details regarding electrochemistry, solar cell device fabrication and characterization are given in the related parts of the results and discussion chapter.

2.2 Equipments

^{1}H and ^{13}C NMR spectra of the synthesized molecules were recorded on Bruker Spectrospin Avance DPX-400 Spectrometer. Spectroelectrochemical studies were conducted by Varian Cary 5000 UV– Vis spectrophotometer. Electrochemical studies were performed via Voltalab 50 potentiostat.

2.3 Synthesis

2.3.1 Synthesis of 2-Furonitrile [43]

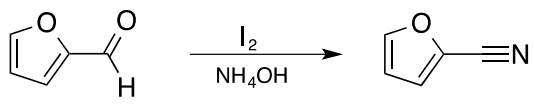

Figure 2.1: Synthetic route of 2 –Furonitrile

Freshley distilled furfural (3.00 g, 31.2 mmol), ammonium hydroxide solution (25%, 264 mL) and THF (31.2 mL) was added into 500 mL reaction flask. The reaction mixture was stirred at room temperature for 5 minutes. After portionwise addition of I_2 (8.71 g, 34.3 mmol) was completed, mixture was stirred about 10 minutes until the faint yellow color of the mixture turned into grey. Then freshly prepared 5% sodium thiosulfate solution (50 mL) poured into reaction flask and the mixture stirred for a few minutes. Then the mixture was extracted with Et_2O. The organic phase was dried over $MgSO_4$ and evaporation of the solvent afforded yellow colored liquid (1.86 g, 64% yield). ^{1}H NMR (400 MHz, $CDCl_3$) δ 7.60 (d, *J* = 2.1 Hz, 1H), 7.13 – 7.09 (m, 1H), 6.55 (dd, *J* = 3.6, 1.8 Hz, 1H). ^{13}C NMR (100 MHz, $CDCl_3$) δ 147.3, 126.2, 122.0, 111.4.

2.3.2 Synthesis of Diethyl Succinate [44]

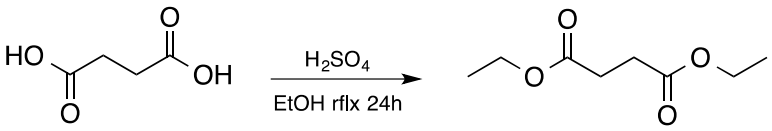

Figure 2.2: Synthetic route of Diethyl Succinate

Ethanol (125 mL), succinic acid (7.38 g, 62.5 mmol), sulphuric acid (3.75 mL) were mixed in two necked-round bottomed 250 mL reaction flask under argon atmosphere. Reaction mixture was stirred for 1 hour at 80 ºC. After the reaction was completed, solvent was removed, water was added and the residue was extracted with Et_2O. The combined organic layer were washed with sat. $NaHCO_3$, dried over $MgSO_4$ and the solvent was evaporated. Product was obtained as a colorless liquid (8.82 g, 80% yield).^{1}H NMR (400 MHz, $CDCl_3$) δ 4.12 (q, *J* = 7.1 Hz, 1H), 2.59 (s, 1H), 1.23 (t, *J* = 7.1 Hz, 1H). ^{13}C NMR (100 MHz, $CDCl_3$) δ 171.8, 60.6, 29.1, 14.1.

2.3.3 Synthesis of 9-(Bromomethyl)nonadecane [45]

Figure 2.3: Synthetic route of 9-(Bromomethyl)nonadecane

9-(Bromomethyl)nonadecane was synthesized from its alcohol precursor. Octyldodecanol (2.0 g, 6.7 mmol), triphenylphosphine (3.56 g, 13.6 mmol) were dissolved in DCM (5 mL) in a two-necked reaction flask under argon atmosphere in room temperature. After the reaction mixture was cooled to 0 °C, NBS (1.78 g, 10.1 mmol) was added in portion wise into reaction medium. Reaction was stirred in room temperature overnight. After the solvent was removed, water was added and the crude product was extracted with hexane (500 mL). The organic layer was dried over ($MgSO_4$) and the solvent wa evaporated. The crude product was purified by column chromatography eluting with hexane (1.95 g, 80% yield).^{1}H NMR (400 MHz, $CDCl_3$) δ 3.45 (d, *J* = 4.7 Hz, 2H), 1.26 (s, 33H), 0.88 (t, *J* = 6.8 Hz, 6H), ^{13}C NMR (100 MHz, $CDCl_3$) δ 39.7, 39.5, 32.5, 31.9, 29.7, 29.6, 29.6, 29.5, 29.3, 29.3, 26.5, 22.6, 14.1

2.3.4 Synthesis of Sodium 3,6-di(furan-2-yl)-1,4-dioxo-1*H*,4*H*-pyrrolo[3,4-*c*]pyrrole-2,5-diide [46]

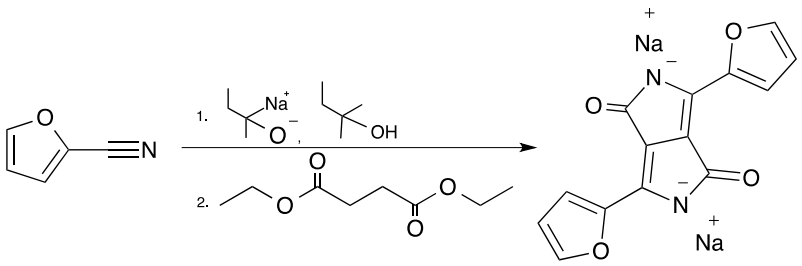

Figure 2.4: Synthetic route Sodium 3,6-di(furan-2-yl)-1,4-dioxo-1*H*,4*H*-pyrrolo[3,4-*c*]pyrrole-2,5-diide

Two necked 100 mL reaction flask was evacuated and filled twice with argon and vacuum cycles. Dry tert- amyl alcohol (50 mL) was injected with a syringe into reaction flask. Reaction was heated up to 75-80 °C and sodium metal (0.50 g, 21.5 mmol) added portionwise until no gas evolution was observed. After all the sodium metals disappeared, temperature of the reaction was raised to 120 ºC and stirred overnight. 2-Furonitrile (2.00 g, 21.5 mmol) was added and reaction was stirred 10 minutes before diethyl succinate (1.255 g, 7.209 mmol) added. Reaction was stirred at 120 ºC for 5 hours while monitoring with TLC. Temperature of the reaction was brought to room temperature and the mixture was filtered through Büchner funnel and washed with MeOH. Powder like solid substance was dried in an one necked flask under reduced pressure. The obtained product was used without any purification in the next step.

2.3.5 Synthesis of 2,5-didodecyl-3,6-di(furan-2-yl)-2,5-dihydropyrrolo[3,4-*c*]pyrrole-1,4-dione [46]

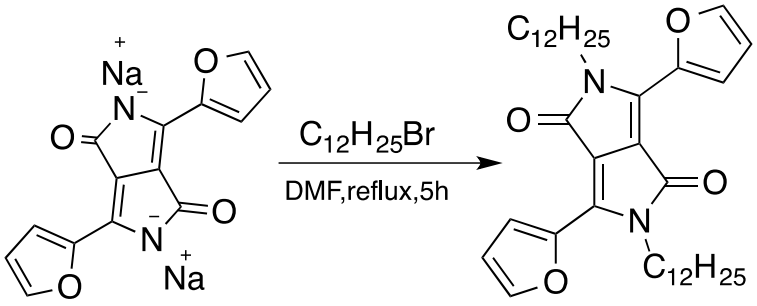

Figure 2.5: Synthetic route of 2,5-didodecyl-3,6-di(furan-2-yl)-2,5dihydropyrrolo[3,4-*c*]pyrrole-1,4-dione

Previously synthesized 3,6-di(furan-2-yl)pyrrolo[3,4-c]pyrrole-1,4(2H,5H)-dione (2.68 g, 8.6 mmol) and dry DMF (39 mL) were charged in a 100 mL two necked reaction flask under argon atmosphere. The mixture was heated to 120 °C and stirred for 30 minutes.1-bromododecane (5.36 g, 21.5 mmol) was introduced to the reaction mixture, temperature was immediately raised to 140 °C and the mixture was stirred

for 5 hours. After the reaction was finished, mixture was precipitated in water, and the precipitate washed with MeOH. The material was collected from filtration flask with $CHCl_3$ and the solvent was evaporated. The residue was purified with column chromatography on silica gel (hexane/$CHCl_3$) two times. The combined yield was 11%, 0.572 g) ^{1}H NMR (400 MHz, $CDCl_3$) δ 8.30 (d, *J* = 3.6 Hz, 2H), 7.63 (d, *J* = 1.3 Hz, 2H), 6.69 (dd, *J* = 3.7, 1.7 Hz, 2H), 4.13 – 4.08 (m, 4H), 1.69 (p, *J* = 7.6 Hz, 4H), 1.27 (d, *J* = 18.3 Hz, 36H), 0.87 (t, *J* = 6.9 Hz, 6H). ^{13}C NMR (100 MHz, $CDCl_3$) δ 160.8, 145.1, 144.6, 133.6, 120.0, 113.4, 106.4, 42.4, 31.9, 30.2, 29.6, 29.6, 29.6, 29.5, 29.3, 29.3, 26.8, 22.6, 14.1.

2.3.6 Synthesis of 3,6-bis(5-bromofuran-2-yl)-2,5-didodesil-2,5-dihydropyrrolo[3,4-*c*]pyrrol-1,4-dione [46]

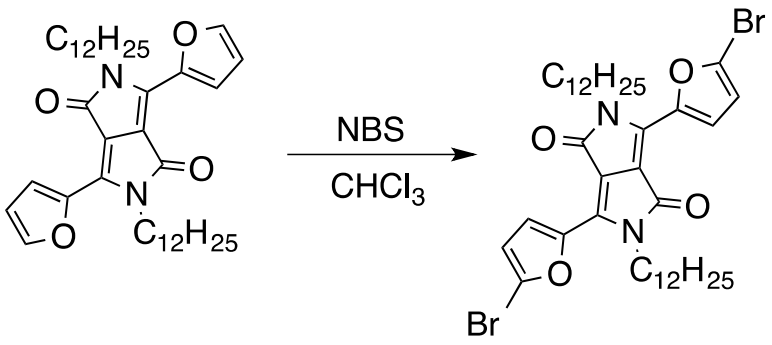

Figure 2.6: Synthetic route of 3,6-bis(5-bromofuran-2-yl)-2,5-didodesil-2,5-dihydropyrrolo[3,4-*c*]pyrrol-1,4-dione

Previously synthesized 2,5-didodecyl-3,6-di(furan-2-yl)-2,5-dihydropyrrolo[3,4-*c*]pyrrole-1,4-dione (1.09 g, 1.80 mmol) and $CHCl_3$ (5 mL) were stirred in a two necked 250 mL reaction flask under argon atmosphere for ten minutes at room temperature. Reaction flask was covered with aluminum foil and protected from light. NBS (0,264 g, 1.48 mmol) was added into reaction slowly and reaction was stirred

for 12 hours at room temperature under dark conditions. After the reaction was completed water was added and the mixture was diluted with $CHCl_3$ and extraction was performed. The organic layers were combined and dried over $MgSO_4$. After the product was concentrated on rotary evaporator, crude product was purified by column chromatography (hexane/ $CHCl_3$) and a dark red color solid was obtained, (0.455 g, 33%) ^1H NMR (400 MHz, $CDCl_3$) δ 8.26 (m, *J* = 2.33 Hz, 2H), 6.63 (m, *J* = 0.98 Hz, 2H), 4.05 (m, *J* = 0.88 Hz, 4H), 1.25 (s, 40H), 0.87 (m, *J* = 0.47 Hz, 6H).

2.3.7 Synthesis of 2,5-bis(trimethylstannyl)-selenophene [47]

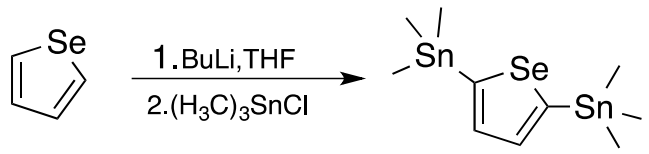

Figure 2.7: Synthetic route of 2,5-bis(trimethylstannyl) -selenophene

Three successive vacuum –argon cycles were applied to a 100 mL two necked reaction flask equipped with stirring bar. Selenophene (1.00 g, 7.63 mmol) was injected with syringe into reaction medium and dry THF (26 mL) was added. Reaction mixture was stirred 10 minutes at room temperature before cooling down to -78 °C. After stirring the reaction at -78 °C for 20 minutes, *n*-BuLi (8mL) was introduced dropwise into the reaction. Upon completion with the addition of *n*-BuLi, reaction stirred at -78 °C for 45 minutes. Then reaction was kept stirring at room temperature for 3 hours. Trimethyltinchloride (18 mL) was introduced into reaction with a syringe and reaction was stirred overnight. The ice-cold water was added and the product was extracted with Et_2O (250 mL). The organic layer was dried over $MgSO_4$, filtrated and the solvent was evaporated under reduced pressure. The residue was recrystalized from ethyl alcohol under argon atmosphere to yield the title compound as white crystals (0.780 g, 24% yield). ^{1}H-NMR (400 MHz, $CDCl_3$, TMS): δ (ppm) 7.60 (s, 2H), 0.31 (s, 18H).

2.3.8 Synthesis of 2,5-didodecyl-3-(5-methylfuran-2-yl)-6-(5-(5 methylselenophen-2-yl)furan-2-yl)-2,5-dihydropyrrolo[3,4-*c*]pyrrole-1,4-dione[48]

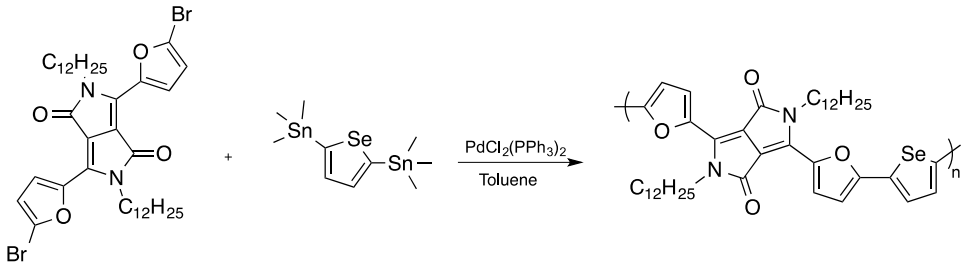

P1

Figure 2.8: Synthetic route of 2,5-didodecyl-3-(5-methylfuran-2-yl)-6-(5-(5-methylselenophen-2-yl)furan-2-yl)-2,5-dihydropyrrolo[3,4-*c*]pyrrole-1,4-dione **(P1)**

3,6-bis(5-bromofuran-2-yl)-2,5-didodecyl-2,5-dihydropyrrolo[3,4-*c*]pyrrole-1,4dione (140 mg, 0.183 mmol) and 2,5-bis(trimethylstannyl)-selenophene (83.56 mg, 0.183 mmol) were mixed in 50 mL schlenk tube which was previously subjected to 3 vacuum-argon cycles. Bis(triphenylphosphine) palladium (II) (5 mol%, 7 mg) were added quickly as a catalyst. Dry toluene (8 mL) was added and reaction was stirred for 24 hours at 95 °C. At the end of the reaction bromobenzene (0.3 mL) was introduced as an end-gapper and the reaction was stirred another 8 hours. Next, tributyl(thiophene-2-yl)stannane (0.25 mL) was added as the other end-gapper. The reaction was stirred for 4 hours additional. After the reaction was completed, solvent was removed and cold MeOH (500 mL) was added and the mixture left overnight to precipitate in the fridge Then, product was filtrated and soxhlet extraction was performed with the following oreder; acetone, hexane and $CHCl_3$. Polymer could not be recovered due to its low solubility.

2.3.9 Synthesis of 3,6-di(furan-2-yl)-2,5-bis(2-octyldodecyl)-2,5-dihydropyrrolo[3,4-*c*]pyrrole-1,4-dione[46]

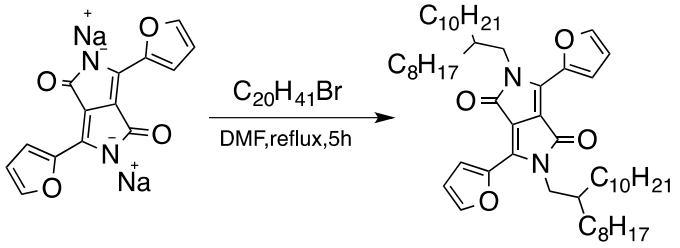

Figure 2.9: Synthetic route of 3,6-di(furan-2-yl)-2,5-bis(2-octyldodecyl)-2,5-dihydropyrrolo[3,4-*c*]pyrrole-1,4-dione

Previously synthesized 3,6-di(furan-2-yl)-1,4-dioxo-1*H*,4*H*-pyrrolo[3,4-*c*]pyrrole-2,5-diide (2.8 g, 9.08 mmol) and dry DMF (40 mL) were charged in a 100 mL two necked reaction flask equipped with condenser and stirring bar, at 120 °C for 30 minutes. 9-(Bromomethyl) nonadecane (9.85 g, 27.3, mmol) was introduced to the reaction and temperature was raised to 140 °C immediately and the mixture was stirred for 5 hours. After the completion of the reaction, DMF was removed, water was addded and extraction was performed with $CHCl_3$. The organic layers were dried over $MgSO_4$. Further purification was achieved with column chromatography using mixture of hexane/ethyl acetate get the 3,6-di(furan-2-yl)-2,5-bis(2-octyldodecyl)-2,5-dihydropyrrolo[3,4-*c*]pyrrole-1,4-dione purple-red solid 2.688 yielded. . ^{1}H NMR (400 MHz, $CDCl_3$) δ 8.26 (d, *J* = 3.6 Hz, 2H), 7.53 (s, 2H), 6.67 – 6.59 (m, 2H), 3.95 (d, *J* = 7.4 Hz, 4H), 1.80 – 1.59 (m, 4H), 1.22 – 1.14 (m, 64H), 0.79 (q, *J* = 7.0, 6.4 Hz, 12H). ^{13}C NMR (100 MHz, $CDCl_3$) δ 161.2, 144.7, 144.6, 133.9, 120.1, 113.4, 106.4, 46.5, 38.5, 31.9, 31.8, 31.4, 30.0, 29.6, 29.5, 29.3, 29.3, 26.5, 22.6, 14.1.

2.3.10 Synthesis of 3,6-bis(5-bromofuran-2-yl)-2,5-bis(2-octyldodecyl)-2,5-dihydropyrrolo[3,4-*c*]pyrrole-1,4-dione [46]

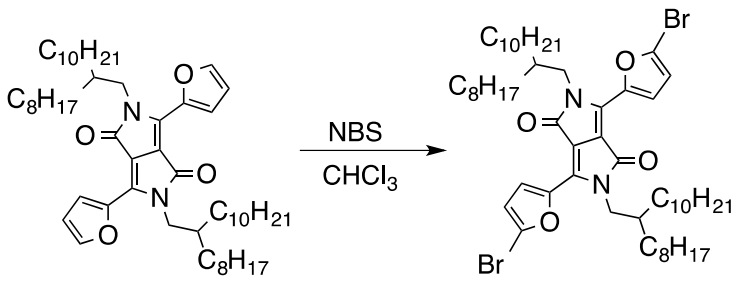

Figure 2.10: Synthetic route of 3,6-bis(5-bromofuran-2-yl)-2,5-bis(2-octyldodecyl)-2,5-dihydropyrrolo[3,4-*c*]pyrrole-1,4-dione

Previously synthesized 3,6-di(furan-2-yl)-2,5-bis(2-octyldodecyl)-2,5-dihydropyrrolo[3,4-*c*]pyrrole-1,4-dione (300 mg, 0.36 mmol) and $CHCl_3$ (5 mL) were introduced into a 250 mL reaction flask under argon atmosphere at room temperature and the mixture was stirred for 10 minutes. Reaction flask was covered with an aluminum foil and NBS (0.135 g, 0.758 mmol) was added portionwise at 0 °C. Reaction was continued to stir for 30 minutes then extracted with $CHCl_3$. The organic layer was dried over $MgSO_4$. After the product was concentrated on rotary evaporator, crude product was purified by column chromatography (hexane/$CHCl_3$) and 3,6-bis(5-bromofuran-2-yl)-2,5-bis(2-octyldodecyl)-2,5-dihydropyrrolo[3,4-*c*]pyrrole-1,4-dione was obtained as a dark red solid yield 40%), 0.141 g.^{1}H NMR (400 MHz, $CDCl_3$) δ 8.30 (d, *J* = 3.7 Hz, 2H), 6.62 (d, *J* = 3.7 Hz, 2H), 3.98 (d, *J* = 7.4 Hz, 4H), 1.79 (s, 2H), 1.23 (s, 62H), 0.86 (s, 14H).

2.3.11 Synthesis of 3-(5-methylfuran-2-yl)-6-(5-(5-methylselenophen-2-yl)furan-2-yl)-2,5-bis(2-octyldodecyl)-2,5-dihydropyrrolo[3,4-*c*]pyrrole-1,4-dione (P2) [48]

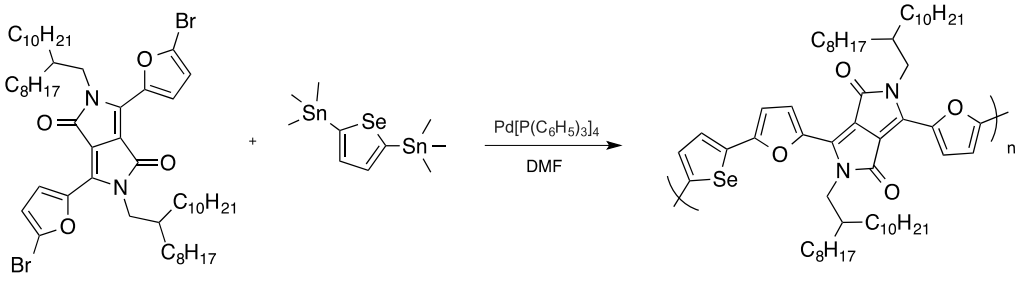

P2

Figure 2.11 Synthetic route of: 3-(5-methylfuran-2-yl)-6-(5-(5-methylselenophen-2-yl)furan-2-yl)-2,5-bis(2-octyldodecyl)-2,5-dihydropyrrolo[3,4-*c*]pyrrole-1,4-dione **(P2)**

A 100 mL flame dried schelenk tube was previously subjected to 3 vacuum-argon cycles before the materials were introduced. Previously synthesized 3,6-bis(5-bromofuran-2-yl)-2,5-bis(2-octyldodecyl)-2,5-dihydropyrrolo[3,4-*c*]pyrrole-1,4-dione (100 mg, 0.101 mmol) and 2,5-bis(trimethylstannyl)-selenophene (46.0 mg, 0.101 mmol) were mixed in a 100 mL schelenk tube under argon atmosphere. Subsequently, tetrakis(triphenylphosphine)palladium(0) (7 mg) was added as a catalyst and dry DMF (8 mL) as the solvent. Temperature was raised to 95 °C and was stirred for 44 hours. After the reaction was completed, the solvent was removed and the product was precipitated in cold MeOH (500 mL). Product was filtered and for further purification with soxhlet extraction was performed in the following order; acetone hexane. The polymer was obtained in hexane phase due to its high solubility.

2.3.12 Synthesis of 3,6-di(furan-2-yl)-2,5-dihydropyrrolo[3,4-*c*]pyrrole-1,4-dione[46,49]

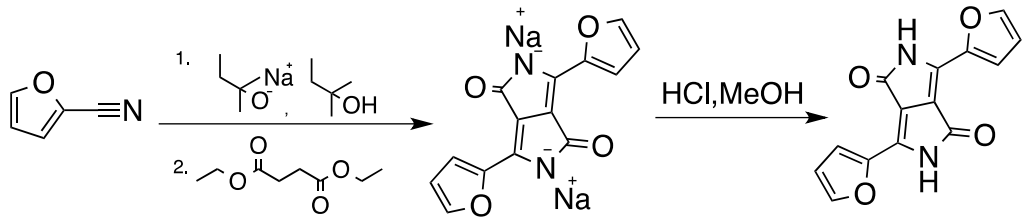

Figure 2.12: Synthetic route of 3,6-di(furan-2-yl)-2,5-dihydropyrrolo[3,4-*c*] pyrrole-1,4-dione

Two necked 50 mL reaction flask equipped with a condenser, was subjected to 3 vacuum-argon cycles before the materials were introduced. Dry tert-amyl alcohol (25 mL) was injected into reaction flask and heated up to 75 °C. Sodium metal pieces (0.249 g, 10.74 mmol) were added in a portion wise manner until the all the sodium metals disappeared and gas evolution stopped. Then temperature was raised to 120 ^{o}C and reaction was stirred overnight. 2-Furonitrile (1.00 g, 10.74 mmol) was added into reaction and stirred for ten minutes and subsequently, diethyl succinate (0.623 g, 3.58 mmol) was added in dropwise. The mixture was stirred for 5 hours at 120 °C. After the reaction was brought to room temperature, crude product was precipitated in a solution of hydrochloric acid (3.2 mL) and MeOH (64 mL). The product was filtrered via Buchner and washed with MeOH under vacuum. Solid product with a dark red color was obtained. (1.73 g, 70% yield). ^{1}H NMR (400 MHz, DMSO-d_6) δ 11.21 (s, 1H), 8.05 (d, J = 2.8 Hz, 1H), 7.68 (d, J = 4.4 Hz, 1H), 6.83 (dd, J = 3.5, 1.7 Hz, 1H), 3.66 (s, 1H). ^{13}C NMR (100 MHz, DMSO) δ 161.1, 146.8, 143.7, 131.2, 116.7, 113.6, 107.5.

2.3.13 Synthesis of 3,6-di(furan-2-yl)-2,5-dioctadecyl-2,5-dihydropyrrolo [3,4-*c*]pyrrole-1,4-dione [46]

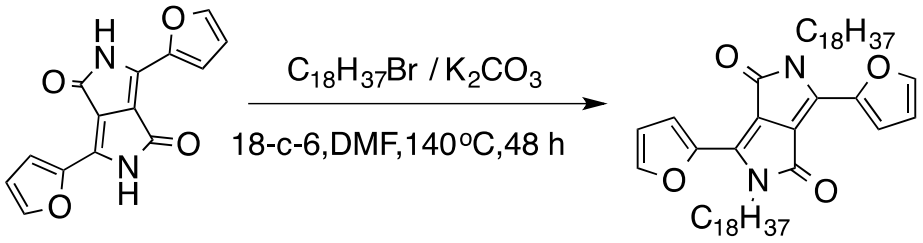

Figure 2.13: Synthetic route of 3,6-di(furan-2-yl)-2,5-dioctadecyl -2,5-dihydropyrrolo[3,4-*c*]pyrrole-1,4-dione

A 50 mL two-necked round bottom flask was evacuated and filled with argon and vaccum cycles twice. Previously synthsized 3,6-di(furan-2-yl)-2,5-dihydropyrrolo[3,4-*c*]pyrrole-1,4-dione (0.609 g, 2.27 mmol), K_2CO_3 (1.35 g, 9.78 mmol), dry DMF (25 mL) and a catalytic amount of 18-crown-6 were added into reaction flask under argon atmosphere. The mixture was stirred in room temperature for ten minutes and temperature was raised to 130 °C and kept stirring at that temperature for 1 hour. 1-bromooctadecane (2.805 g, 8.401 mmol) was added into reaction portion-wise. The reaction was stirred at 130°C for 48 hours. After the reaction was completed, solvent was removed. Sticky crude product was extracted with $CHCl_3$ (300 mL), dried over $MgSO_4$ and filtered. After the evaporation of the solvent product was purified with column chromatography on silica gel (2:1 hexane/DCM, and the target compound was attained as a dark red solid (0.453 g, 25 %). ^{1}H NMR (400 MHz, $CDCl_3$) δ 8.30 (d, *J* = 3.6 Hz, 2H), 7.63 (d, *J* = 1.4 Hz, 2H), 6.69 (dd, *J* = 3.7, 1.7 Hz, 2H), 4.13 – 4.07 (m, 4H), 1.73 – 1.66 (m, 4H), 1.32 – 1.22 (m, 60H), 0.87 (t, *J* = 6.8 Hz, 6H). ^{13}C NMR (100 MHz, $CDCl_3$) δ 160.8, 145.0, 144.7, 133.6, 120.0, 113.4, 106.4, 42.4, 31.9, 30.2, 29.6, 29.6, 29.5, 29.3, 29.2, 26.8, 22.6, 14.0. HRMS calcd. for $C_{50}H_{81}N_2O_4$: 773.6196, found 773.6205.

2.3.14 Synthesis of 3,6-bis(5-bromofuran-2-yl)-2,5-dioctadecyl-2,5-dihydropyrrolo[3,4-*c*]pyrrole-1,4-dione [46]

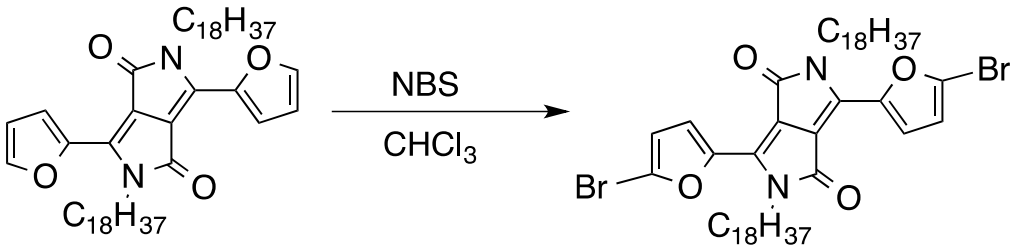

Figure 2.14: Synthetic route of 3,6-bis(5-bromofuran-2-yl)-2,5-dioctadecyl-2,5-dihydropyrrolo[3,4-*c*]pyrrole-1,4-dione

A 50 mL two-necked flask was evacuated and filled with argon twice and previously synthesized 3,6-di(furan-2-yl)-2,5-dioctadecyl-2,5-dihydropyrrolo[3,4-*c*]pyrrole-1,4-dione (0.409 g, 0.528 mmol) and $CHCl_3$ (10 mL) was added into reaction flask under argon atmosphere. Reaction flask was covered with aluminum foil and NBS (0.280 g, 1.58 mmol) was added into reaction in one portion. Reaction was stirred for 12 hours under dark. Water was added and the mixture was extracted with $CHCl_3$ several times. Combined organic phases were dried, over $MgSO_4$. After the solvent was removed further purification performed with column chromatography on silica gel 3:2 hexane/$CHCl_3$) was performed to get the 3,6-bis(5-bromofuran-2-yl)-2,5-dioctadecyl-2,5-dihydropyrrolo[3,4-*c*]pyrrole-1,4-dione as a resulted dark purple-red solid (100 mg, 20%). ^{1}H NMR (400 MHz, $CDCl_3$) δ 8.25 (d, *J* = 111.4, 3.3 Hz, 2H), 6.63 (d, *J* = 3.6 Hz, 2H), 4.08 – 4.02 (m, 4H), 1.55 (dd, *J* = 95.9, 25.9 Hz, 64H),0.88 (t, *J* = 6.7 Hz, 9H). ^{13}C NMR (100 MHz, $CDCl_3$) δ 160.5, 146.2, 132.5, 126.3, 126.2, 121.9, 115.4, 106.4, 42.5, 31.8, 30.1, 29.7, 29.2, 26.8, 22.5, 13.9. HRMS calcd. for $C_{50}H_{79}N_2O_4Br_2$: 929.4407, found 929.4407.

2.3.15 Synthesis of 3-(5-methylfuran-2-yl)-6-(5-(5-methylselenophen-2-yl)furan-2-yl)-2,5-dioctadecyl-2,5-dihydropyrrolo[3,4-*c*]pyrrole-1,4-dione (P3) [50]

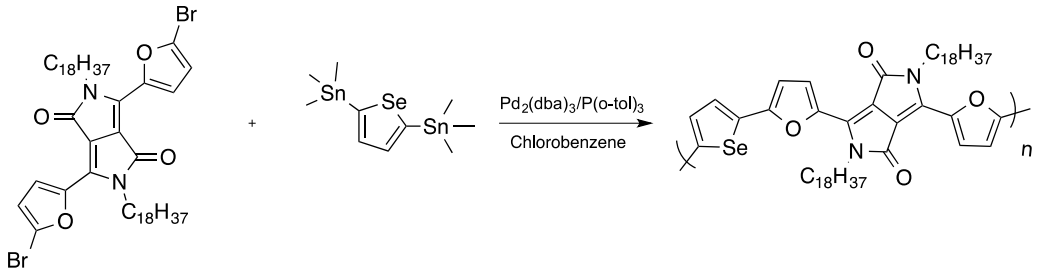

P3

Figure 2.15: Synthetic route of 3-(5-methylfuran-2-yl)-6-(5-(5-methylselenophen-2-yl)furan-2-yl)-2,5-dioctadecyl-2,5-dihydropyrrolo[3,4-c]pyrrole-1,4-dione **(P3)**

A 50 mL Schlenk tube under argon atmosphere 3,6-bis(5-bromofuran-2-yl)-2,5-dioctadecyl-2,5-dihydropyrrolo[3,4-*c*]pyrrole-1,4-dione (165 mg, 0.177 mmol) and 2,5-bis(trimethylstannyl)-selenophene (80 mg, 0.177 mmol), were added and the reaction was put under argon. Chlorobenzene (6 mL) was injected with a syringe and solution was degassed by bubbling the argon with cannula for 30 minutes. Then, tris(dibenzylideneacetone)dipalladium(0) (2 mol%) and tris(*o*-tolyl)phosphine (8 mol%) were added to the solution and schlenk tube was put in oil bath which was heated at 90 °C. The reaction mixture was stirred at 90 °C for 5 minutes and then temperature was raised to 110 °C and stirred for 24 hours. Reaction was monitored with TLC in 24^{th} hour and additional catalysts tris(dibenzylideneacetone)dipalladium(0) (4 mol%) and tris(*o*-tolyl)phosphine (16 mol%) were introduced into reaction. The mixture stirred for additional 12 hours. The reaction was cooled to room temperature and diluted with $CHCl_3$ (5 mL) and as a palladium scavenger, sodium diethylditiocarbamate trihydrate (5.0 g) added and the mixture was stirred for 1 hour. The resulting mixture was precipitated into cold methanol (200 mL). After filtration, the product was purified with Soxhlet extraction, washed with methanol, hexane and finally with $CHCl_3$ to yield 153 mg of the target

polymer. Number-average (Mn) and weight-average (Mw) molecular weight were determined by Agilent Technologies 1200 series GPC running in chlorobenzene at 80 ^{o}C, using two PL mixed B columns in series, and calibrated against narrow polydispersity polystyrene standards. Number-average (Mn) and weight-average (Mw) molecular weight was found as 4.6 kDa and 50.3 kDa, respectively.

CHAPTER III

RESULTS AND DISCUSSION

3.1 Synthesis

During this study, by changing the side chains of the DPP cored polymer, the optimum solubility, film forming ability and ideal morphology for active layer was aimed. In our initial followed reaction pathway, DPP salt reaction was used without any further purification and it was expected to put the alkyl side chain C_{12} linear in one step as it was proposed in the literature. Our first synthesized polymer had a poor solubility in common organic solvents, including orthodichlorobenzene. Thus, we are unable to carry out the solar cell studies. In our second polymer synthesis, we decided to use a branched alkyl chain in order to overcome solubility obstacle we utilized a an alkyl chain which is commomnly used in the literature. We polymerized branched alkyl chain containing DPP monomer selenophene using two different catalysts and polymerization conditions, using tetrakis(triphenylphosphine)palladium(0) in DMF 48 hour, 95 ^{o}C and presence of bis(triphenylphosphine)palladium(II) dichloride in toluene 24 hour, 95 ^{o}C. Former one showed poor film forming characteristics while the second one has good optical absorption and film forming properties however poor poewer conversion efficiency results were obtained (<%1). Third monomer was synthesized with C_{18} linear alkyl chain which provided the optimum solubility results. In the synthesis of the DPP core with C_{18} alkyl chain, we preferred to protonate the DPP salt and purify it [33]. This approach provided several advantages. The most important one was to start the next step, alkylation, with a pure precusor and knowing the exact amount and ratios for reagents. However, we had issues in the synthesis and purification of this material when we followed the literature procedures. We needed to make modifications from the literature because proposed methods in the literature;

precipating in alcohol using the glacial acid did not work. Throughout the synthesis of furan based DPP molecules, although the reactions were simple, purifications via column chromatography were the most difficult part. The purification of synthesized molecules, for both alkylation and bromination steps, required several columns which resulted in comparatively low yields. Due to low solubility of P1 no further studies were conducted.

3.2 Cyclic Voltammetry

In order to calculate the electronic band gap of the polymers and to determine the highest occupied molecular orbital (HOMO) and the lowest unoccupied molecular orbital (LUMO) energy levels, cyclic voltammetry studies were conducted. Polymers were dissolved in $CHCl_3$ (5 mg/mL) and applied as a thin layer onto ITO coated glass surfaces via spray coating method. The cyclic voltammetry measurements were carried out in three-electrode system immersed in 0.1 M $TBAPF_6$ in acetonitrile (ACN) solution. The three-electrode system consisted of the polymer coated ITO or polymer coated platinum (Pt) as the working electrode, platinum (Pt) wire as the counter electrode and the silver wire (Ag) served as the reference electrode. For the scan rate of 100 mV/s, p- and n- dopable properties were observed during the oxidation and reduction process. Below equations were used for calculating the LUMO and HOMO energy levels from the onset potentials of reduction and oxidation peaks.

$$\mathrm{HOMO} = -(4.75 + \mathrm{E}_{\mathrm{onset}}^{\mathrm{ox}})$$
$$\mathrm{LUMO} = -(4.75 + \mathrm{E}_{\mathrm{onset}}^{\mathrm{red}})$$

The cyclic voltammetry spectra of **P2** is shown in Figure 3.1. The p-type and n-type reversible oxidation and reduction pairs of **P2** were observed. Since **P2** is ambipolar, the band gap of polymers can be calculated from CV directly. The measured HOMO from onset of oxidation peak is -5.48 for **P2**. The LUMO was calculated as -3.70. Difference of HOMO and LUMO levels of corresponding polymer electronic band gap (E_g^{ec}) calculated as 1.78 eV for **P3**. These results are summarized in Table 3.1. The optical bandgap was calculated from the onset and was found to be 1.34 eV for **P3**. Cyclic voltammogram of P3 was also recorded and from the onset of oxidation

and reduction potentials the HOMO and LUMO levels were calculated at 5.46 eV and 3.81 eV respectively. Electronic band gap of the polymer was calculated as 1.65 eV from the difference between HOMO and LUMO energy levels.

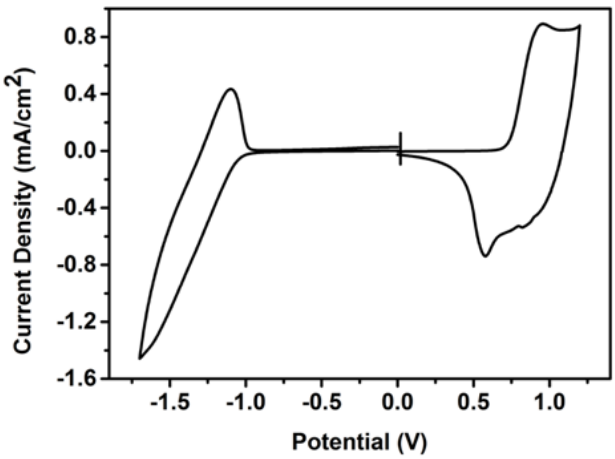

Figure 3.1: Cyclic Voltammetry for **P2**

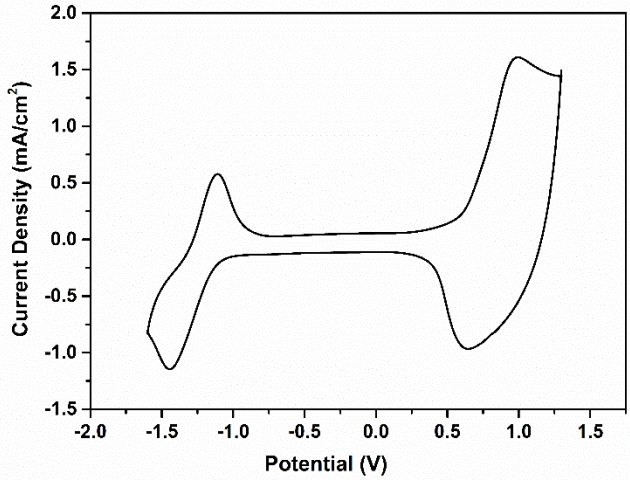

Figure 3.2: Cyclic Voltammetry for **P3**

Table 3.1: Summary of the photovoltaic properties of **P2** and **P3**

	$E_{pdoping}$ (V)	$E_{p\text{-}dedoping}$ (V)	$E_{n\text{-}doping}$ (V)	$E_{n\text{-}dedoping}$ (V)	HOMO (eV)	LUMO (eV)	E_g^{ec} (eV)	λmax (nm)	E_g^{op} (eV)
P2	0.95	0.58	-1.60	-1.09	-5.48	-3.70	1.78	722/383	1.37
P3	0.99	0.64	-1.45	-1.10	-5.46	-3.81	1.65	880/927	1.34

3.3 Spectrochemical Studies

In this study, spectroelectrochemical experiments were performed to investigate the optical properties of polymers during redox reactions. Polymer films were prepared in $CHCl_3$ solution (5 mg/mL) and then spray coated on the ITO coated glass. Measurements were conducted in three-electrode system in the presence of acetonitrile and $TBAPF_6$ as a solvent and supporting electrolyte couple. The spectroelectrochemical spectra of **P2** in UV-Vis and NIR region is shown in figure 3.2. Maximum at 383 nm and 722 nm refers π-π* transition of the polymer both in the visible region. During the stepwise oxidation, while the absorption peak at 722 nm diminishes, polaron and bipolaron bands appear. While the color of the **P2** was green-blue in neutral state it has changed into grey at 1.1 volt where it's fully oxidized state. The spectroelectrochemical spectra of **P3** in UV-Vis and NIR region is shown the figure 3.4. Maximum at 880 nm and 927 nm refers to absorption in near IR region.

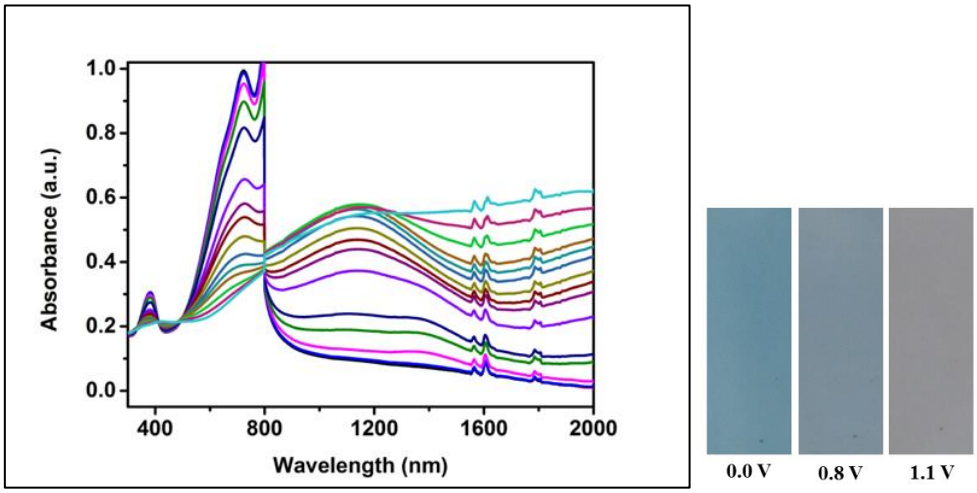

Figure 3.3: UV–Vis–NIR absorption spectra of **P2**

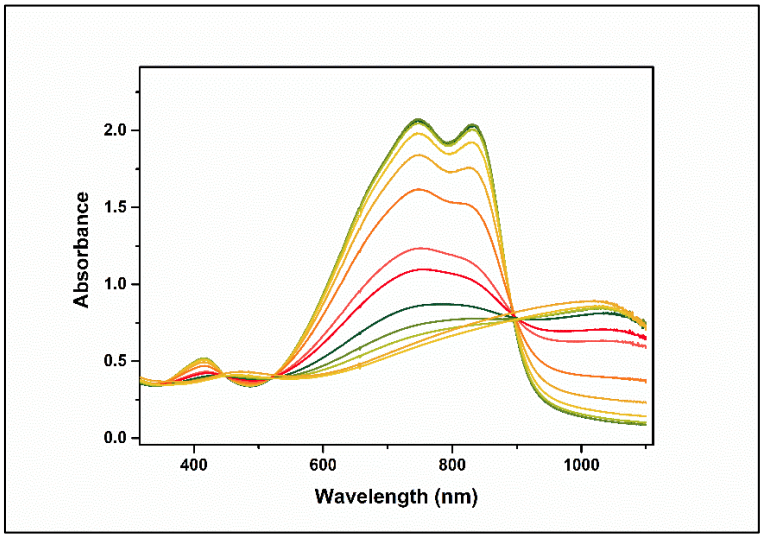

Figure 3.4: UV–Vis–NIR absorption spectra of **P3**

3.4 Kinetic Studies

Kinetic studies were conducted in order to investigate the percent transmittance while the potentiostat scans the neutral and oxidized states with applied potential square wave. Switching time is the time required for transition between colored state and bleached state of the electrochromic material at 95% optical contrast. Measurements were concucted by applying square-wave potential within a 5 s time intervals at maximum absorption wavelength values obtained in visible and near IR regions. The optical contrast was calculated for 40% at 720 nm, 49% at 1160 nm and 66% at 1850 nm for **P2**. Switching times are 1.5 s, 3.4 s and 2.1 s respectively. The optical contrast change in the visible region is one of the highest reported value for a DPP based polymer.

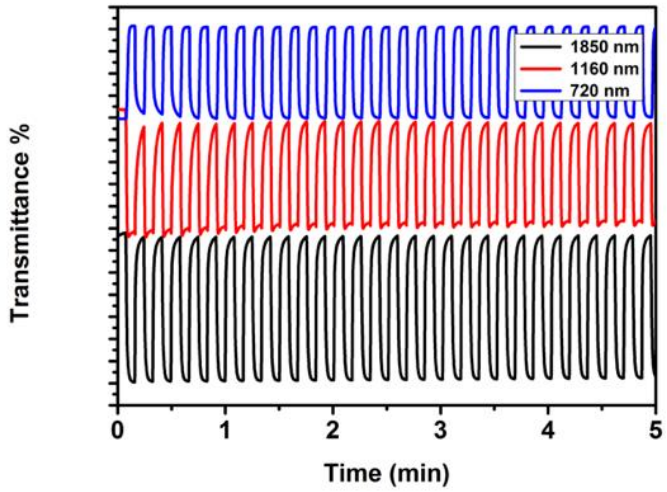

Figure 3.5: Percent Transmittance Change of **P2**

Applied voltage was changed between 0.0-1.3V for **P3** in defined time interval and the percent transmittance was measured in visible and near IR regions. The results for optical contrast of **P3** was measured as 38% at 745 nm, 35% at 830 nm and 47% at 1035 nm.

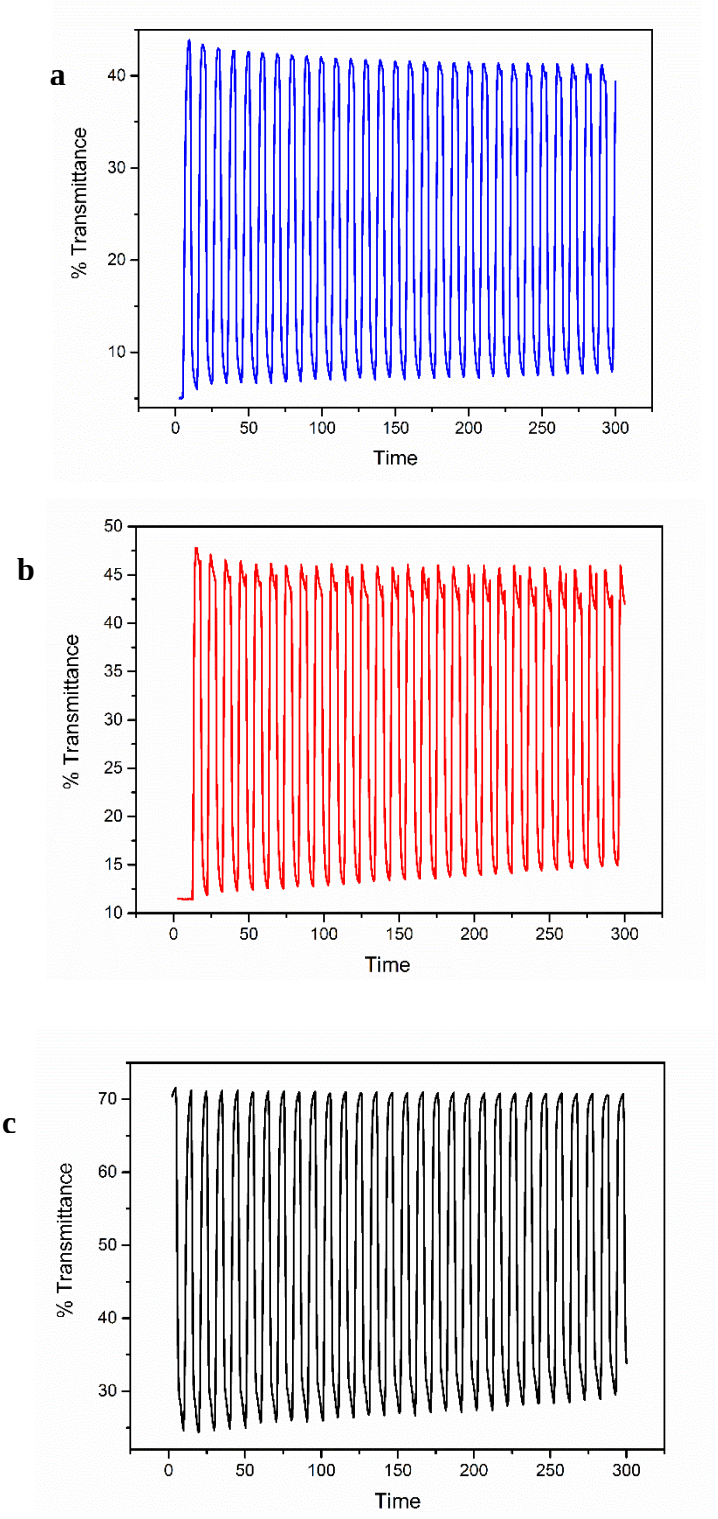

Figure 3.6: Percent Transmittance Change of **P3**

(a) 745nm (b) 830 nm (c) 1035 nm

3.5 Organic Solar Cell Applications

3.5.1 Bulk Heterojunction Solar Cell Application

Due to low solubility of P1 no studies were performed of solar cell applications. In order to investigate photovoltaic properties of P2, different optimization conditions were studied with the ITO/PEDOT:PSS/polymer:$PC_{71}BM$/LiF/Al device structure. ITO coated glass substrates were cleaned by touluene, detergent, water and isopropyl alcohol in ultrasonic bath and dried with N_2 gun. Before a thin layer of PEDOT:PSS (~40 nm) layer was spin coated, oxygen plasma treatment was applied in order to minimize surface contaminatation and improve the work function of ITO [51]. The substrates were heated at 135 ^oC for 15 minutes. P2 and $PC_{71}BM$ were blended in different ratios in orthodichloro benzene solution with 10 mg/mL concentration and filtered through PTFE filter. Then active layer was coated with spin coater with different speeds in order to find out the optimum active layer thickness. A thin layer of LiF (1nm) and aluminum (10 nm) were coated by thermal evaporation. For decided device structure which was ITO/PEDOT:PSS/polymer:$PC_{71}BM$/LiF/Al, **P2** and $PC_{71}BM$ were blended in 1:2, 1:3, and 1:4 ratios in toluene and chlorobenzene and different coating speeds, 750 rpm and 1000 rpm. However results were obtained less than 1% efficiency. The device fabricated from **P3** exhibited significantly improved results when compared with **P2**. **P3** and $PC_{71}BM$ was blended at different ratios in *o*-DCB and applied as active layer in bulk heterojunction solar cell device. The preferred device architecture is ITO/PEDOT:PSS/polymer:$PC_{71}BM$/LiF/Al. The measurements were made in glove box filled with N_2 under AM 1.5G irradiation (100 mW/cm^2). For optimized conditions, polymer-$PC_{71}BM$ ratios (1:3) and spin coating speed, the best power conversion efficiency (PCE) was found as 3.00 % and exhibited an open circuit voltage (V_{OC}) of 0.6 V, short circuit current (J_{SC}) of 7.95 mA/cm^2 and a fill factor (FF) of 0.63.

In this study the additive effect in normal bulk heterojunction solar cell applications was also investigated. In the normal device structure as mentioned above, the additives did not improve the results in any significant way.

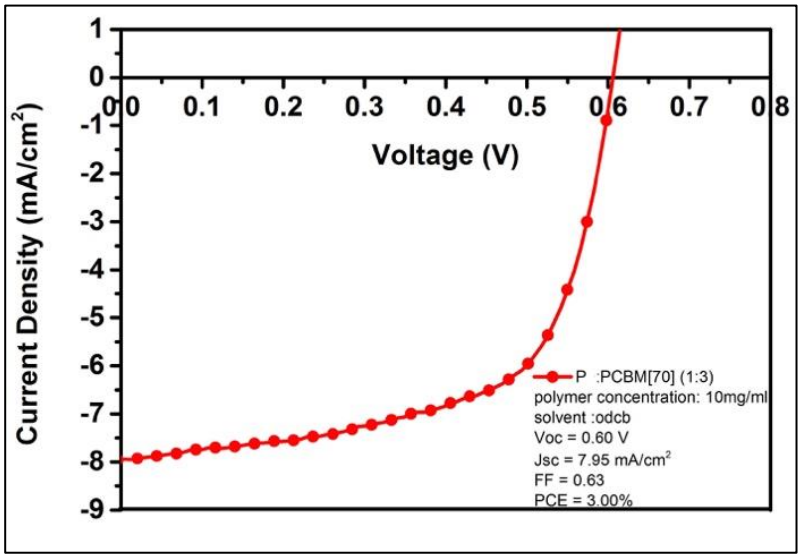

Figure 3.7: Current density–voltage curves of the optimized for ITO/PEDOT:PSS/P3:$PC_{71}BM$/LiF/Al

3.5.2 Inverted Organic Solar Cell Applications

In collaboration with Baran Group at KAUST, inverted solar cells were fabricated with a device structure of ITO/ZnO/P3:$PC_{71}BM$/MoO_x/Ag. The solar cells were preapared on ITO (15 Ω sq^{-1}) coated glass substrates with device area 0.1 cm^2. Substrates were cleaned with dilute Extran 300 detergent solution to remove organic residues before immersing in an ultrasonic bath of dilute Extran 300 for 20 min. Samples were rinsed in flowing deionized water for 5 min before being sonicated (Branson 5510) for 10 min each in successive baths of acetone and isopropanol. Next, the samples were dried with pressurized nitrogen before being exposed to a UV−ozone plasma for 20 min. The ZnO precursor solution was prepared according to established procedures, and was spin-cast at 3000 rpm onto the ITO-coated glass substrates and baked at 150 °C for 15 min in air. Immediately after baking the substrates, the samples were then transferred into a dry nitrogen glovebox (< 3 ppm

O^2) for active layer deposition. All solutions were prepared in the glovebox using the polymer donors, and $PC_{71}BM$ (purchased from Nano-C). P3 and $PC_{71}BM$ were dissolved in chlorobenzene without any solvent additive, and the solutions were stirred overnight at 60 °C hotplate. Several optimizations the thickness, additive ratio and blend ratio were investigated. The best devices were prepared using P3:$PC_{71}BM$ ratio of 1:3 (by weight), with an overall concentration of 20 mg mL^{-1}. The active layers were spin-cast from the solutions in a glove box at 400 rpm for 30 sec, resulting in a film of ~185 nm in thickness. The samples were placed in a thermal evaporator for evaporation of of a 5 nm thick molybdenium oxide (MoO_3) layer and a 100 nm thick layer of silver, at a pressure of less than $2x10^{-6}$ Torr. Following electrode deposition, samples underwent J−V testing. J-V measurements of solar cells were performed in the glovebox with a Keithley 2400 source meter and an Oriel Sol3A Class AAA solar simulator calibrated to 1 sun, AM1.5 G, with a KG-5 silicon reference cell certified by Newport. The external quantum efficiency (EQE) measurements were performed at zero bias by illuminating the device with monochromatic light supplied from a Xenon arc lamp in combination with a dual-grating monochromator. The number of photons incident on the sample was calculated for each wavelength by using a silicon photodiode calibrated by NIST. Table 3.2 was corresponded to optimization details of donor/ acceptor ratio of **P3** and $PC_{71}BM$ in chlorobenzene solution with 20 mg/mL concentration spin coated with 2000 rpm forming 95 nm thick layer. The best result for **P3** to $PC_{71}BM$ ratio was found as 1:3.

Table 3.2: Photovoltaic Performance of **P3** with different **P3**:$PC_{71}BM$ ratios

P3:$PC_{71}BM$ Ratio	Jsc (mA/cm^2)	Voc (V)	FF	PCE (%)
1:1	0.78	0.56	33.2	0.15
1:2	1.89	0.63	54.6	0.65
1:3	2.22	0.63	62.8	0.93
1:4	2.05	0.64	58.6	0.77
1:5	1.85	0.61	52.1	0.59

Next the effect of additive was investigated. As summarized in table Table 3.3**,** here very interesting results were obtained. With 3% diphenyl ether (DPE) additive PCE of the cells increased dramatically. With the optimization of film thickness via changing concentration of the polymer:PCBM solution and rotation speed for the spin coating, a high efficiency of 6.16% (average 6.02% over six devices) was achieved. The optimum film thickness was found to be 210 nm. It is important to note here that a high FF was achieved with a thick active layer which is rare on organic solar cells. To be able make a clear comparison, devices with optimized conditions were prepared with no additive and results are given below:

Table 3.3: Comparison of photovoltaic performance of **P3** with 3 % DPE additive

	Jsc(mA/cm^2)	**Voc (V)**	**FF**	**PCE (%)**	**Average PCE***
CB	1.66	0.63	50.0	0.52	0.47
CB+ 3%DPE	16.0	0.64	60.4	6.16	6.02

The additive result in almost 13 fold increase in the PCE. The one of the highest enhancements using DPE as an additive. EQE data for devices were also recorded and the integrated J_{sc} data (1.50 mA/cm^2 and 15.4 mA/cm^2) was consistent with actual J_{sc} data (1.66 mA/cm^2 and 16.0 mA/cm^2) from the devices. Strong contribution is achieved from the NIR region where EQE values were in order of 45 % between 700 nm and 850 nm. (Table 3.3 and Figure 3.8 and Figure 3.9)

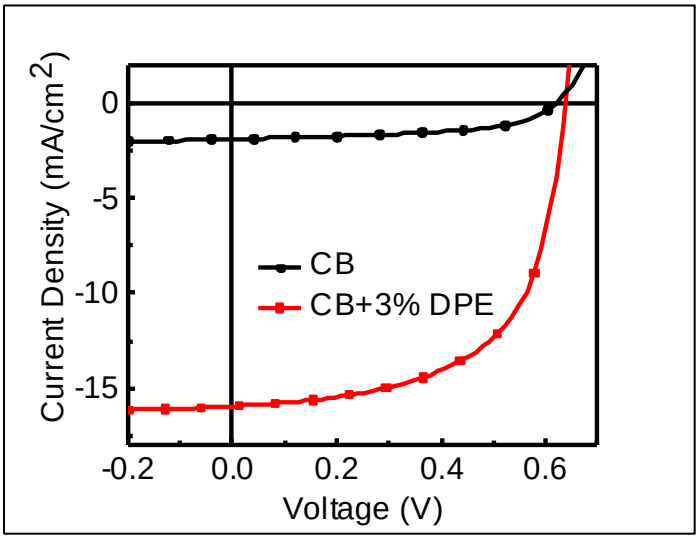

Figure 3.8: Current density–Voltage characteristics of P3 with and without 3 % DPE additive

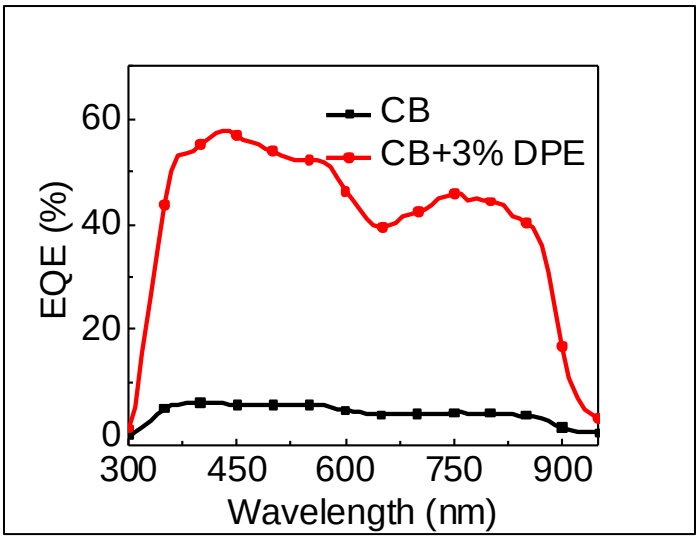

Figure 3.9: EQE spectra of P3 with/without 3% DPE

In order to see the effect of additive on morphology morphology A 5400 Agilent atomic force microscope AFM was used to image the active layers in tapping mode (topography and phase images are represented below). Active layers have root-mean-square (rms) roughness of 1.62 nm and 2.92 nm respectively. With 3% DPE into the film, the $PC_{71}BM$ become dispersed, and DPP polymer form perfect nanofiber with a

diameter of several ten nanometer, which is beneficial for the exciton separation and carrier transfer. Without additive, there are very big domain sizes, which means strong aggregation of $PC_{71}BM$ and significant phase separation. This morphology is not optimal for carrier generation and transfer (Figure 3.10 and Figure 3.11).

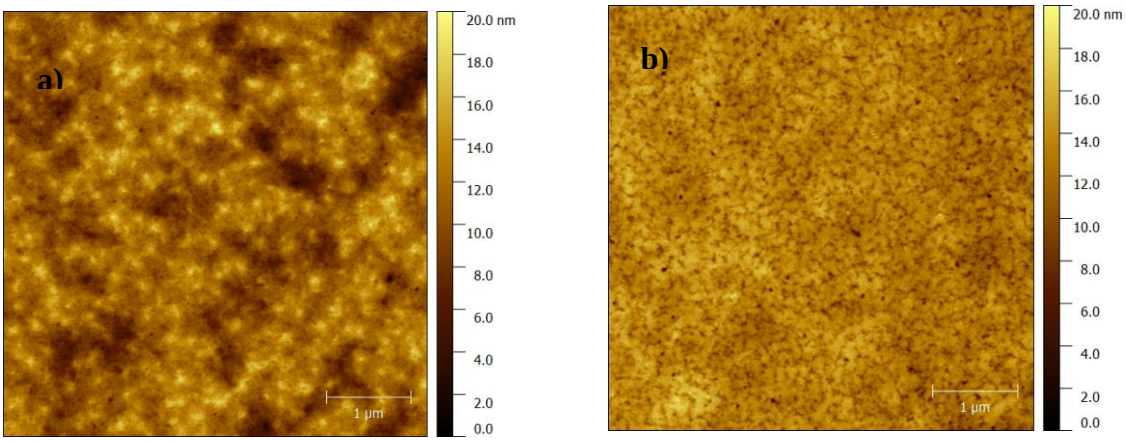

Figure 3.10: AFM images of P3: $PC_{71}BM$ (1:3) Topography images (a) CB without additive (b) CB with 3 %DPE

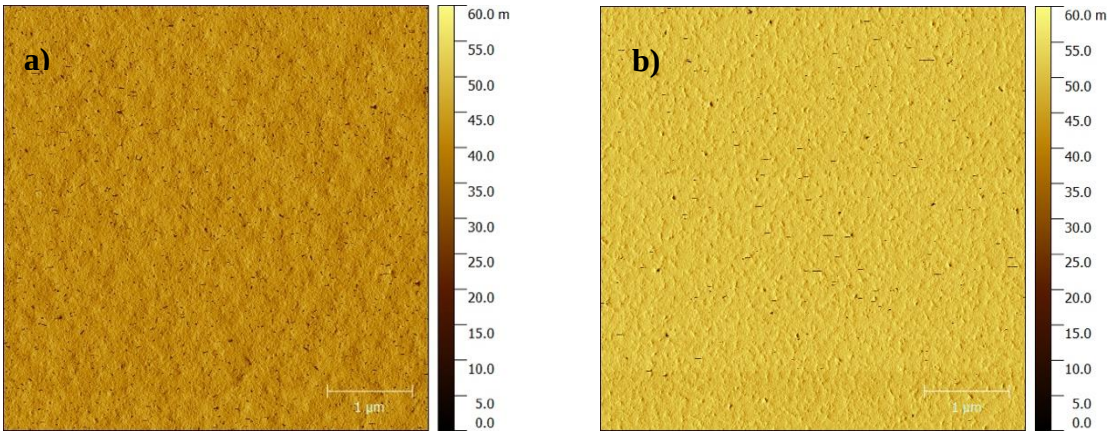

Figure 3.11: AFM images of P3: $PC_{71}BM$ (1:3) Phase images (a) CB without additive (b) CB with 3 %DPE

For further understanding of additive effect in active layer, TEM analyses were also performed. TEM images were recorded in bright field mode with a microscope operating at 300 keV (Tecnai Bio twin, FEI), using an 4k x 4k eagle CCD camera(FEI). Similar to the pattern of AFM images, we also observe strong aggregation of $PC_{71}BM$ in the film without additive. The morphology have a significant change when DPE is added into the film. The favorable nanoscale phase separation benefited the charge generation and transport, and thus high J_{SC} and FF was obtained (Figure 3.12).

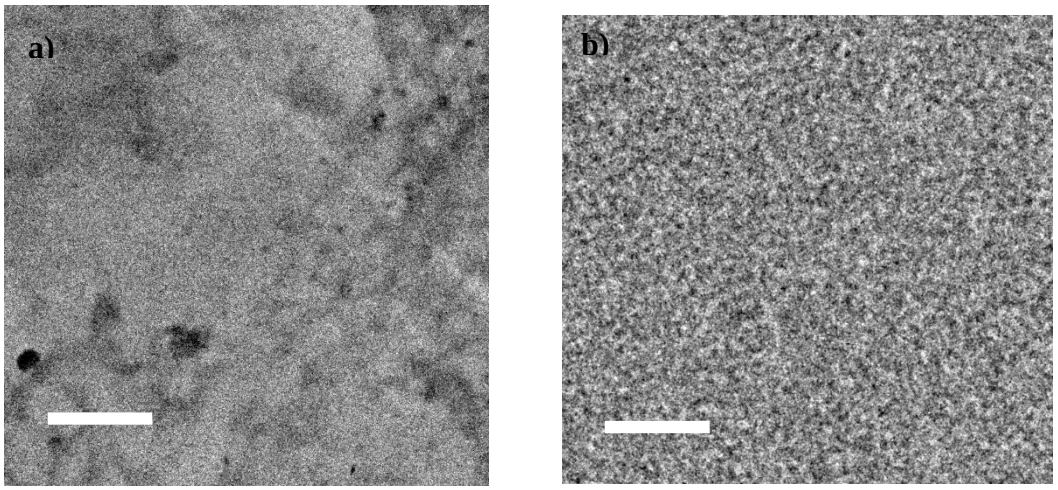

Figure 3.12: TEM images of **P3:** $PC_{71}BM$ (a) without DPE (b) with 3% DPE

In addition to AFM and TEM studies the effect of additive of charge carrier properties were also investigated. Because of the big domain size and $PC_{71}BM$ nanoclusters formed in the film when no additives were introduced electron mobility is much higher than hole mobility. From AFM and TEM images, DPE has significant assistance to tune the morphology and phase separation, so PCBM domains become much smaller and polymer donors form nanofiber matrix, which means polymer crystallization is improved.

in photocurrent [52]. In our study space charge limited current (SCLC) measurements performed to investigate charge carrier mobilities. Hole mobility of the blend films were employed with the architecture ITO/PEDOT:PSS/Polymer/MoO_x/Ag. At the same time, electron mobilities of blend films were utilized with the architecture: ITO/ZnO/Active layer/Ca/Al. Hole mobilities were calculated using Eqn. 1:

$$J_{SCL}=\frac{9}{8}\varepsilon_o\theta\varepsilon_r\mu\frac{V^2}{L^3} \qquad \text{(Eqn 1)}$$

Where ε is the dielectric permittivity of the polymer (generally taken to be about 3), ε_0 is the dielectric permittivity of free space, L is the film thickness (185 nm in this case), and V is the voltage, which is defined as $V = V_{appl}-V_{bi}$, where V_{appl} is the applied voltage, V_{bi} is the built-in voltage which is related to the difference in the work function of the electrodes. Results were summairzed in Table 3.4, we concluded that even the electron mobility slightly decreased upon addition of DPE, hole mobility exhibited significant increase.

Therefore hole/electron mobility have more potential to be balanced, which is beneficial for the FF improvement. (Figure 3.13).

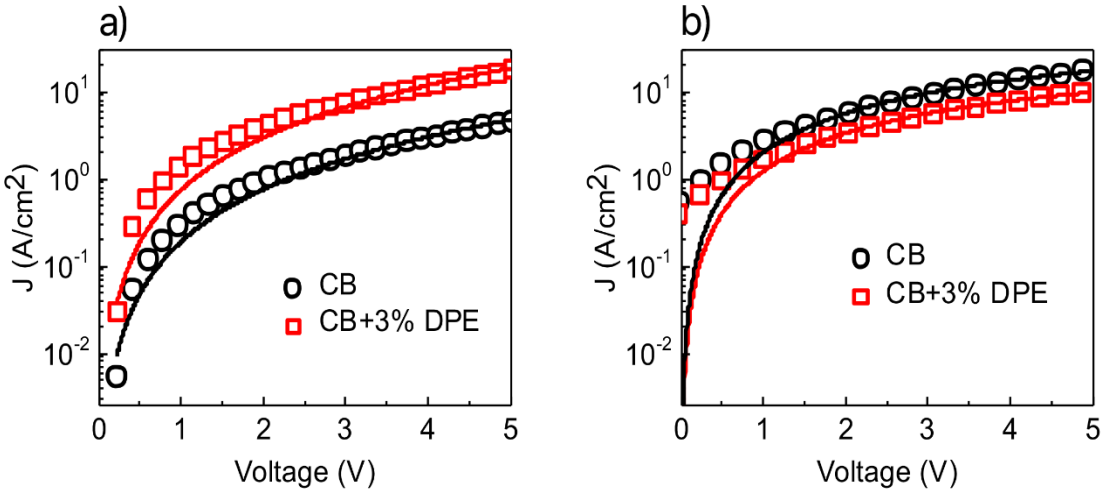

Figure 3.13: a) Hole mobilities of **P3** spin coated from CB and from CB+3%DPE **b)** Electron mobilities of **P3** spin coated from CB and from CB+3%DPE

Table 3.4: Comparison of the charge mobilities of P3 with/without 3 % DPP

	Hole mobility (cm^2/ V s)	Electron mobility (cm^2/ V s)	Ratio
CB	3.52×10^{-5}	3.21×10^{-4}	9.12
CB+ 3% DPE	3.44×10^{-4}	2.68×10^{-4}	0.78

In table 3.5 we reported our final results for P3 in this study. From all the optimization studies we obtained best device performance with ITO/ZnO/P3:PCBM/MoOx/Ag architecture with P3:PCBM ratio (1:3), concentration: 30 mg/mL in presence of 3% DPE additive with active layer thickness 210 nm with spin coating speed 400 rpm.

Table 3.5: Summary of the photovoltaic properties of **P3**

	Jsc (mA/cm^2)	Voc (V)	FF	PCE (%)	Av. PCE (%)
CB	1.66	0.63	50.0	0.52	0.47
CB+3% DPE	16.0	0.64	60.4	6.16	6.02

CHAPTER V

CONCLUSION

In this study, three different poymers were synthesized with using three different alkyl chains on the acceptor unit which are 2,5-didodecyl-3-(5-methylfuran-2-yl)-6-(5-(5-methylselenophen-2-yl)furan-2-yl)-2,5-dihydropyrrolo[3,4-*c*]pyrrole-1,4-dione (P1), 3-(5-methylfuran-2-yl)-6-(5-(5-methylselenophen-2-yl)furan-2-yl)-2,5-bis(2-octyldodecyl)-2,5 dihydropyrrolo[3,4-*c*]pyrrole-1,4-dione (P2), 3-(5-methylfuran-2-yl)-6-(5-(5-methylselenophen-2-yl)furan-2-yl)-2,5-dioctadecyl-2,5-dihydropyrrolo[3,4-*c*]pyrrole-1,4-dione (**P3**). All three polymers were designed according to D-A approach aimed to have strong absorption in the near IR region. It was shown that all polymers absorbs strongly in the Near IR region. Dodecane side chain on P1 did not provide enough solubility for polymer in order to investigate solar cell studies. Branched alkyl chain on **P2** exhibit good electrochromic and optoelectronic properties. In bulk heterojunction solar cell applications of **P2** with ITO/PEDOT:PSS/P2:$PC_{70}BM$/LiF/Al device structure, PCEs lower than 1% was obtained **P3** also showed promising electrochromic properties. 38% optical contrast was attained in the visible region. Best photovoltaic results were obtained with **P3** with linear C_{18} alkyl side chain 1-bromooctadecane. Both convential BHJ solar cell application and inverted-structure solar cell applications of **P3** were investigated in presence of additive effect. In conventional BHJ application, additives of DIO and DPE up to 5% showed no further improvements in device performance. This result may be the reason that the morphology of the active layer had already been fine-tuned on PEDOT:PSS layer. Photovoltaic study result for P3 with ITO/PEDOT:PSS/P3:$PC_{71}BM$/LiF/Al (1:3) device structure showed power conversion efficiency of 3.00 %. Inverted solar cell application with ITO/ZnO/P3:$PC_{71}BM$/MoO_x/Ag device structure, PCE of P3 increased from 0.47% to 6.02% (average) in presnce of 3% DPE additive. AFM and TEM analysis proved the significant change in morphology, better nanoscale phase separation and better

crsytal domains which in turn enhanced the charge transport. V_{oc} of 0.64 V, J_{sc} value of 16.0 mA/cm^2 and FF of 60.4% are the complementary results of the highest PCE observed for **P3** in inverted structure which was 6.16% and this is among the highest reported PCEs for DPP based polymers. The polymer is one of the rare examples of a material that shows promising properties as both electrochromic and solar cell material.

REFERENCES

[1] Perlin, J. (2013). *Let it Shine: The 6,000-Year Story of Solar Energy*. Novato, California: New World Library

[2] World Energy Council. (2016, September 4). World Energy Resources Bioenergy 2016. Retrieved from World Energy Council website: https://www.worldenergy.org/wpcontent/uploads/2017/03/WEResources_Bioenergy_2016.pdf

[3] Glunz, S., Preu, R., & Biro, D. (2012) 1.16: Crystalline Silicon Solar Cells. State-of-the-Art and Future Developments, *Compherensible Renewable Energy,* 353-387

[4] Kalogirou, S. (2014), *Solar Energy Engineering Processes and Systems*. Amsterdam; Boston: Elsevier, AP, Academic Press is an imprint of Elsevier, 2014

[5] Green, M. A. (2007). *Journal of Materials Science: Materials in Electronics*, *18* (SUPPL. 1), 15–19.

[6] Ghahremani, A., & Fathy, A. E. (2016). *Energy Science & Engineering*, *4* (5), 334–343.

[7] Martin,R. (2016, March 3) Sustainable Energy, First Solar's Cells Break Efficiency Record. Retrieved from https://www.technologyreview.com/s/600922/first-solars-cells-break-efficiency-record/

[8] Fang, Z., Wang, X. C., Wu, H. C., & Zhao, C. Z. (2011). *International Journal of Photoenergy*, *(1)*.

[9] Morales-Acevedo, A. (2006). *Solar Energy*, *80* (6), 675–681.

[10] Park, N. G. (2015). *Materials Today*, *18*(2), 65–72.

[11] Burschka, J., Pellet, N., Moon, S.-J., Humphry-Baker, R., Gao, P., Nazeeruddin, M. K., & Grätzel, M. (2013). *Nature*, *499*(7458), 316–319.

[12] Sun, S., & Sariciftci, N.S. (2005). Organic photovoltaics:mechanism, materials and devices. Boca Raton, FL: Taylor & Francis.

[13] Brabec, C.J., Dyakonov, V., Parisi, J., & Sariciftci N.S. (Eds.). (2003).*Organic Photovoltaics: Concepts and Realization.*Germany: Springer-Verlag.

[14] Günes, S., Neugebauer, H., & Sariciftci, N. S. (2007). *Chemical Reviews*, *107* (4), 1324–1338.

[15] Lu, L., Zheng, T., Wu, Q., Schneider, A. M., Zhao, D., & Yu, L. (2015). *Chemical Reviews*, *115*(23), 12666–12731.

[16] Brabec, C. J., Sariciftci, N. S., & Hummelen, J. C. (2001). *Advanced Funtional Materials*, *11*(1), 15–26.

[17] Sariciftci, N. S. (1999). *Current Opinion in Solid State and Materials Science*, *4*(4), 373–378.

[18] Chen, Y.-J., Yang, S.-H., & Hsu, C.-S. (2009). *Chem.Rev.*, *109*, 5868.

[19] Tamai, Y., Ohkita, H., Benten, H., & Ito, S. (2015). *Journal of Physical Chemistry Letters*, *6* (17), 3417–3428.

[20] Dou, L., Liu, Y., Hong, Z., Li, G., & Yang, Y. (2015). *Chemical Reviews*, *115* (23), 12633–12665.

[21] Yamamoto, T., Zhou, Z. H., Kanbara, T., Shimura, M., Kizu, K., Maruyama, T., Sasaki, S. (1996). *Journal of the American Chemical Society*, *118* (43), 10389–10399.

[22] Lai, T. H., Tsang, S. W., Manders, J. R., Chen, S., & So, F. (2013). *Materials Today*, *16*(11), 424–432

[23] Litzov, I., & Brabec, C. J. (2013). *Materials*, *6*(12), 5796–5820.

[24] Choy, Wallace C.H. (2013). *Organic Solar Cells: Materials and Device Physics* [Google Books version]. Retrieved from https://books.google.com.tr/books?id=Z-CMj1qE1sUC&printsec=frontcover&redir_esc=y#v=onepage&q&f=false

[25] Shirakawa, T., Umeda, T., Hashimoto, Y., Fujii, A., Katsumi, Y. (2004). *Journal of Physics D. Applied Physics, 37* (6), 847.

[26] Nho, S., Baek, G., Park, S., Lee, B. R., Cha, M. J., Lim, D. C., … Cho, S. (2016).. *Energy Environ. Sci.*, *9*(1), 240–246.

[27] Tang, A., Zhan, C., Yao, J., & Zhou, E. (2017). *Advanced Materials*, *29* (2).

[28] Tamayo, A. B., Walker, B., & Nguyen, T. Q. (2008). *The Journal of Physical Chemistry C*, *112* (30), 11545-11551

[29] Wienk, M. M., Turbiez, M., Gilot, J. and Janssen, R. A. J. (2008), *Advanced Materials*, 20: 2556–2560

[30] Grzybowski, M., & Gryko, D. T. (2015). *Advanced Optical Materials*, *3*(3), 280–320.

[31] Kyaw, A. K. K., Wang, D. H., Luo, C., Cao, Y., Nguyen, T. Q., Bazan, G. C., & Heeger, A. J. (2014). *Advanced Energy Materials*, *4* (7).

[32] Liao, H. C., Ho, C. C., Chang, C. Y., Jao, M. H., Darling, S. B., & Su, W. F. (2013). *Materials Today*, *16*(9), 326–336.

[33] Yiu, A. T., Beaujuge, P. M., Lee, O. P., Woo, C. H., Toney, M. F., Frechet. (2011). *Journal of American Chemical Society*, *134*, 2180–2185.

[34] Scharber, M. C.; Mühlbacher, D.; Koppe, M.; Denk, P.; Waldauf, C.; Heeger, A. J.; Brabec, C. J. (2006) *Advanced Materials,* 18: 789

[35] Lou, S. J., Szarko, J. M., Xu, T., Yu, L., Marks, T. J., & Chen, L. X. (2011). *Journal of the American Chemical Society*, *133*(51), 20661–20663.

[36] Zhou, H., Zhang, Y., Seifter, J., Collins, S. D., Luo, C., Bazan, G. C., … Heeger, A. J. (2013). *Advanced Materials*, *25*(11), 1646–1652.

[37] Zusan, A., Gieseking, B., Zerson, M., Dyakonov, V., Magerle, R., & Deibel, C. (2015). *Scientific Reports*, *5*(1), 8286

[38] Lee, J. K., Ma, W. L., Brabec, C. J., Yuen, J., Moon, J. S., Kim, J. Y., … Heeger, A. J. (2008). *Journal of the American Chemical Society*, *130*(11), 3619–3623

[39] Pivrikas, A., Neugebauer, H., & Sariciftci, N. S. (2011). *Solar Energy*, *85*(6), 1226–1237

[40] Choi, H., Ko, S.-J., Kim, T., Morin, P.-O., Walker, B., Lee, B. H., … Heeger, A. J. (2015). *Advanced Materials*, *27*(21), 3318–3324.

[41] Lu, L., Zheng, T., Wu, Q., Schneider, A. M., Zhao, D., & Yu, L. (2015). *Chemical Reviews*, *115*(23), 12666–12731

[42] Saadeh, H. A.; Lu, L.; He, F.; Bullock, J. E.; Wang, W.; Carsten, B.; Yu, L. (2012). *ACS Macro Letters*, 1, 361−365.

[43] Upadhyay, S., Chandra, A., & Singh, R. M. (2009). *Chem Inform*, *40*(24).

[44] Moumne, Roba, Solange Lavielle, and Philippe Karoyan. (2006). *The J. Org.Chem., 71,* 3332-3334.

[45] Scheuble, M., Gross, Y. M., Trefz, D., Brinkmann, M., López Navarrete, J. T., Ruiz Delgado, M. C., & Ludwigs, S. (2015). *Macromolecules*, *48*(19), 7049 -7059.

[46] Yiu, A. T., Beaujuge, P. M., Lee, O. P., Woo, C. H., Toney, M. F., Frechet. (2011). *Journal of American Chemical Society*, *134*, 2180–2185.

[47] Kim, K. H., Park, S., Yu, H., Kang, H., Song, I., Oh, J. H., & Kim, B. J. (2014). *Chemistry of Materials*, *26*(24), 6963–6970.

[48] Sonar, P., Singh, S. P., Williams, E. L., Li, Y., Soh, M. S., & Dodabalapur, A. (2012). *J. Mater. Chem.*, *22*(10).

[49] Yiu, A. T., Beaujuge, P. M., Lee, O. P., Woo, C. H., Toney, M. F., & Fréchet, J. M. J. (2012). *Journal of the American Chemical Society*, *134*(4), 2180–2185.

[50] Chen, M. S., Lee, O. P., Niskala, J. R., Yiu, A. T., Tassone, C. J., Schmidt, K., … Fréchet, J. M. J. (2013). *Journal of the American Chemical Society*, *135*(51), 19229–19236.

[51] Ke, J. C., Wang, Y. H., Chen, K. L., & Huang, C. J. (2016). *Journal of Colloid and Interface Science*, *465*, 311–315.

[52] Li, G., Shrotriya, V., Huang, J., Yao, Y., Moriarty, T., Emery, K., & Yang, Y. (2005). *Nature Materials*, *4*(11), 864–868

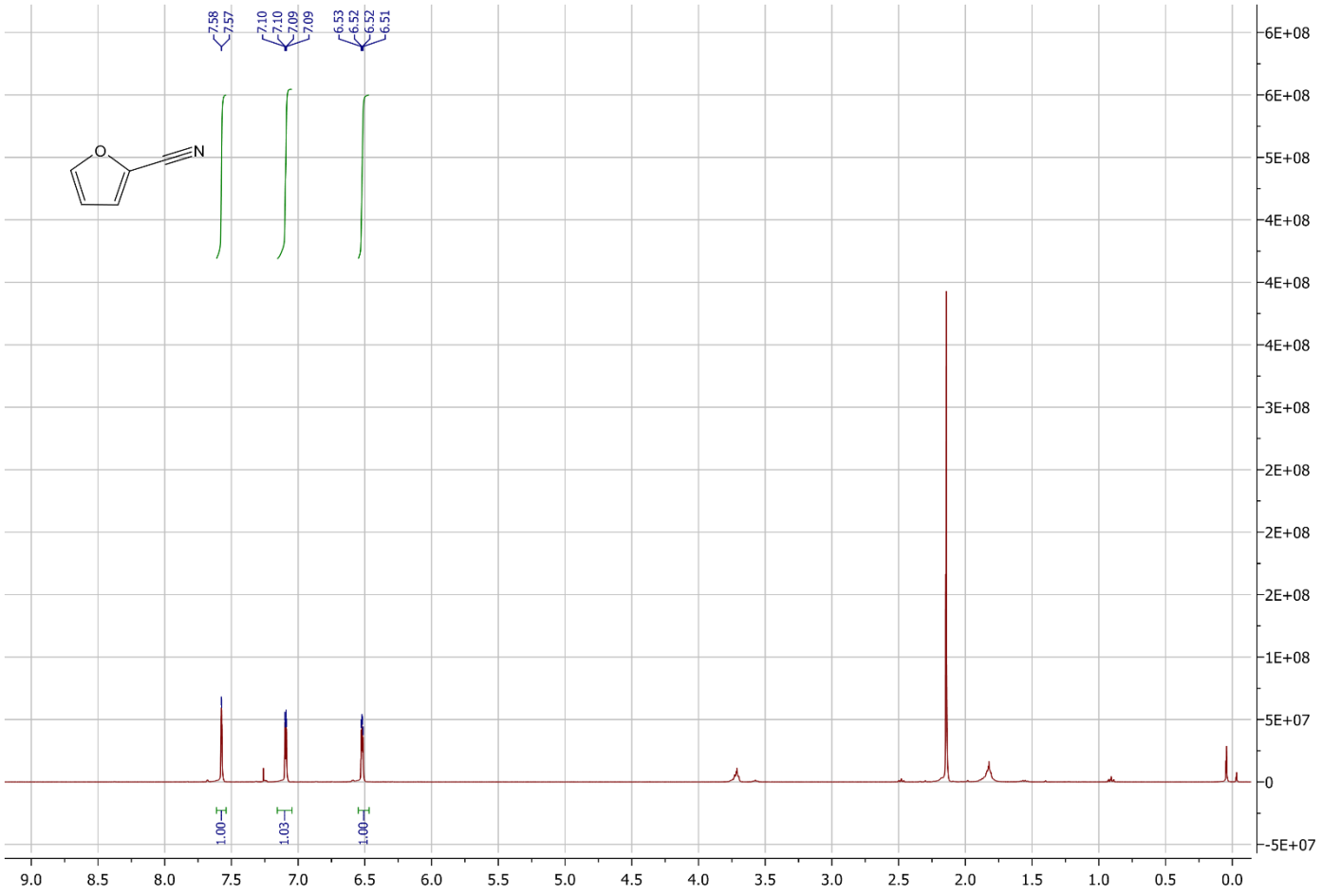

Figure A.1. [1]H-NMR spectrum of 2 –Furonitrile

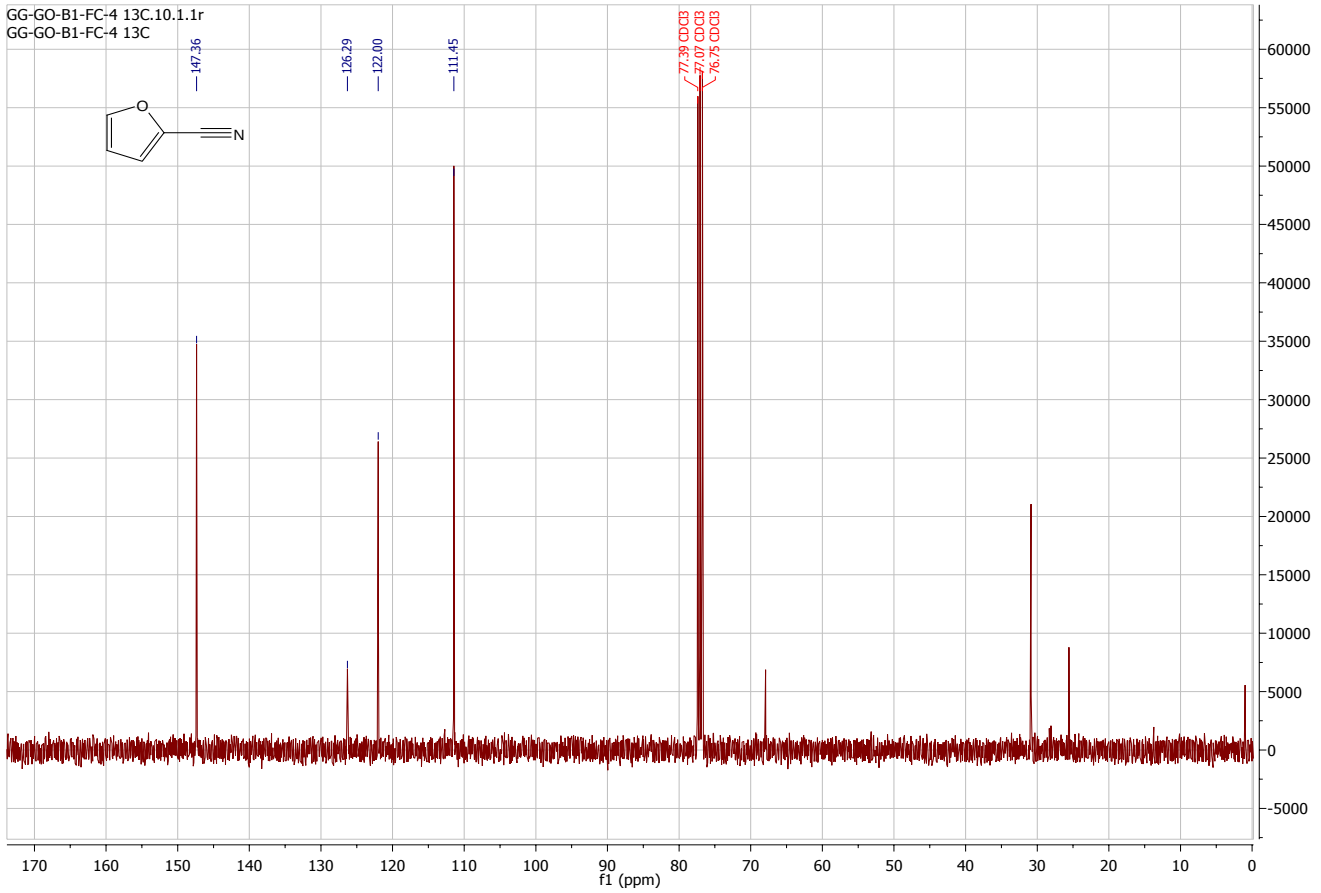

Figure A.2. ^{13}C-NMR spectrum of 2 –Furonitrile

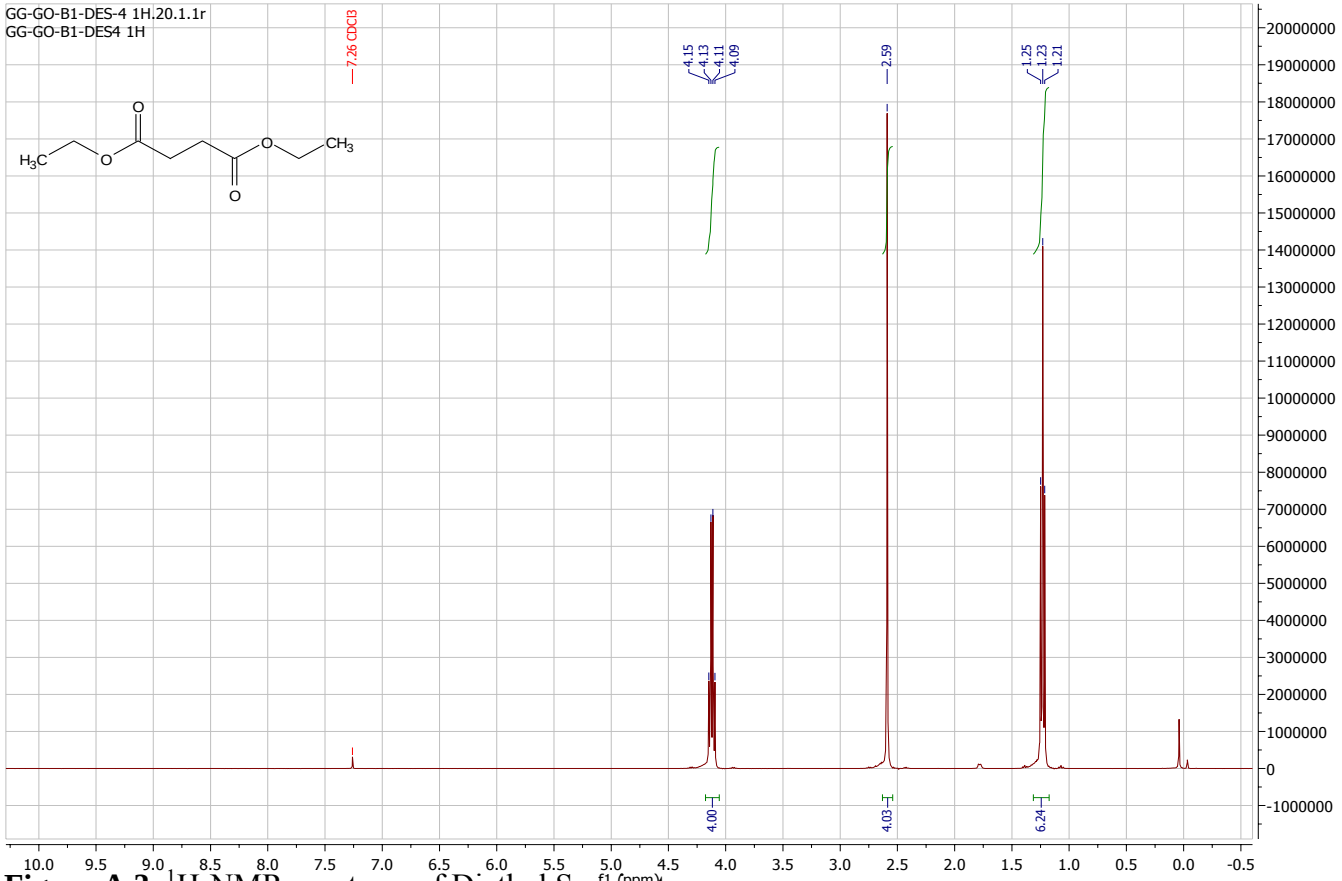

Figure A.3. ^{1}H-NMR spectrum of Diethyl Succinate

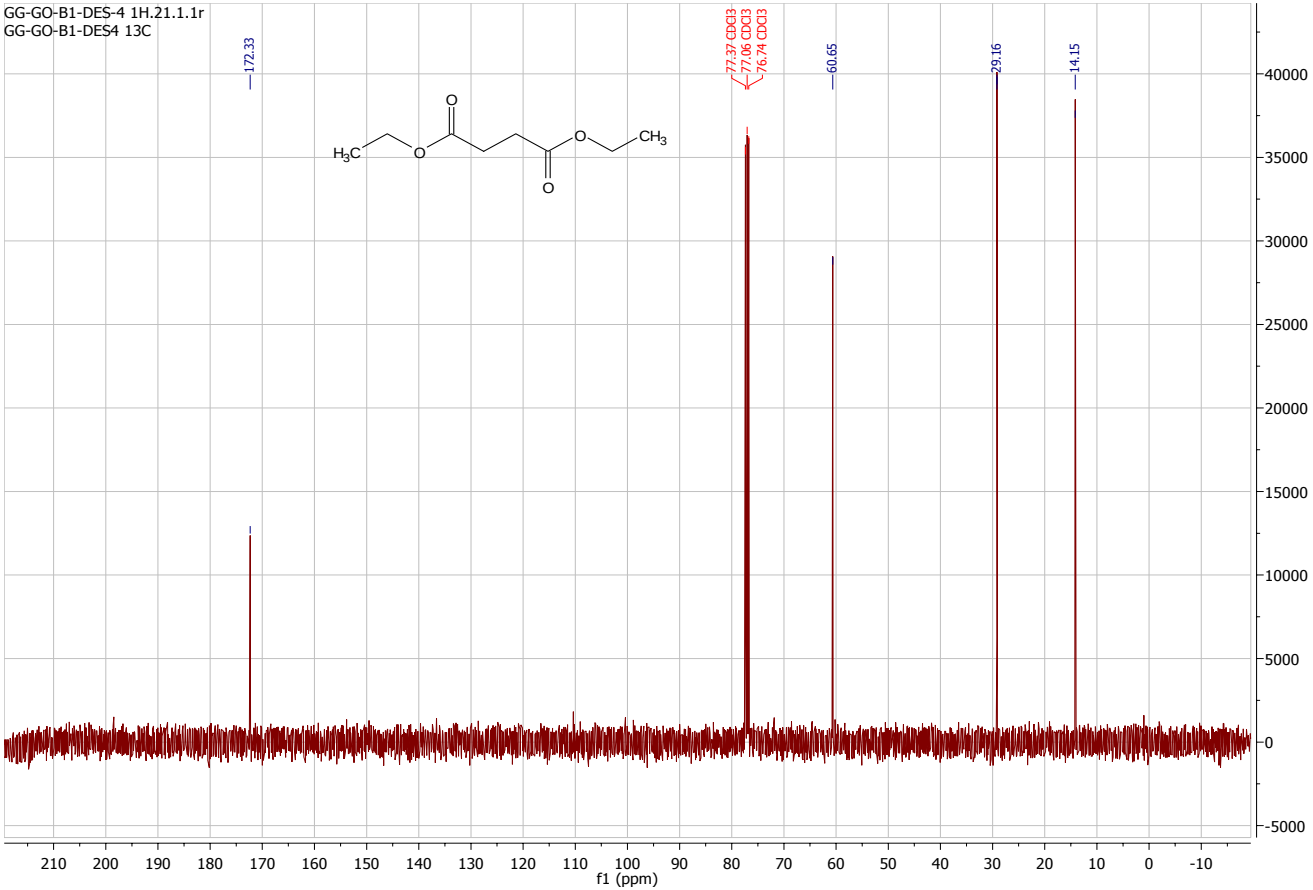

Figure A.4. ^{13}C-NMR spectrum of Diethyl Succinate

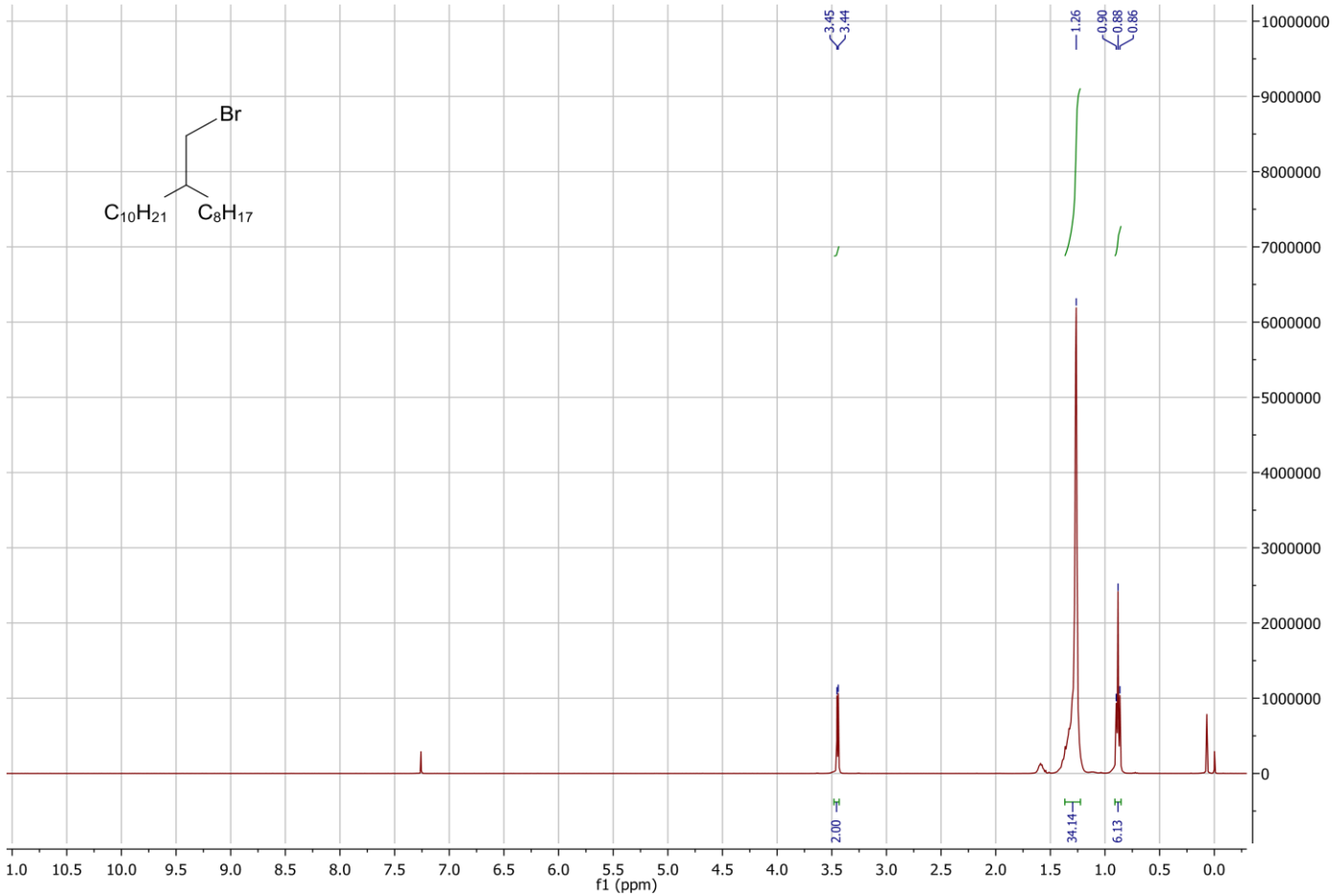

Figure A.5. ^{1}H-NMR spectrum of 9-(Bromomethyl)nonadecane

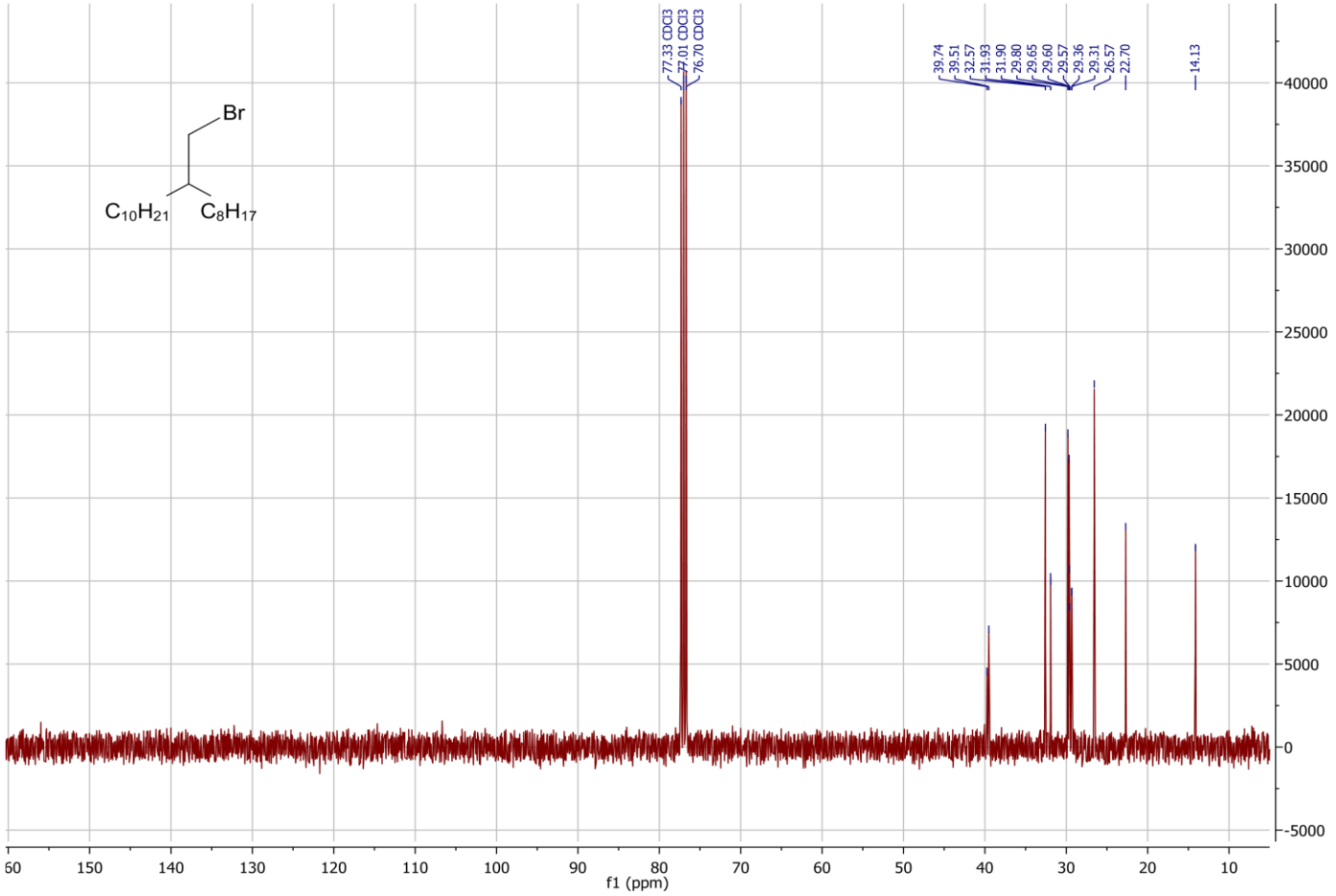

Figure A.6 ^{13}C-NMR spectrum of 9-(Bromomethyl)nonadecane

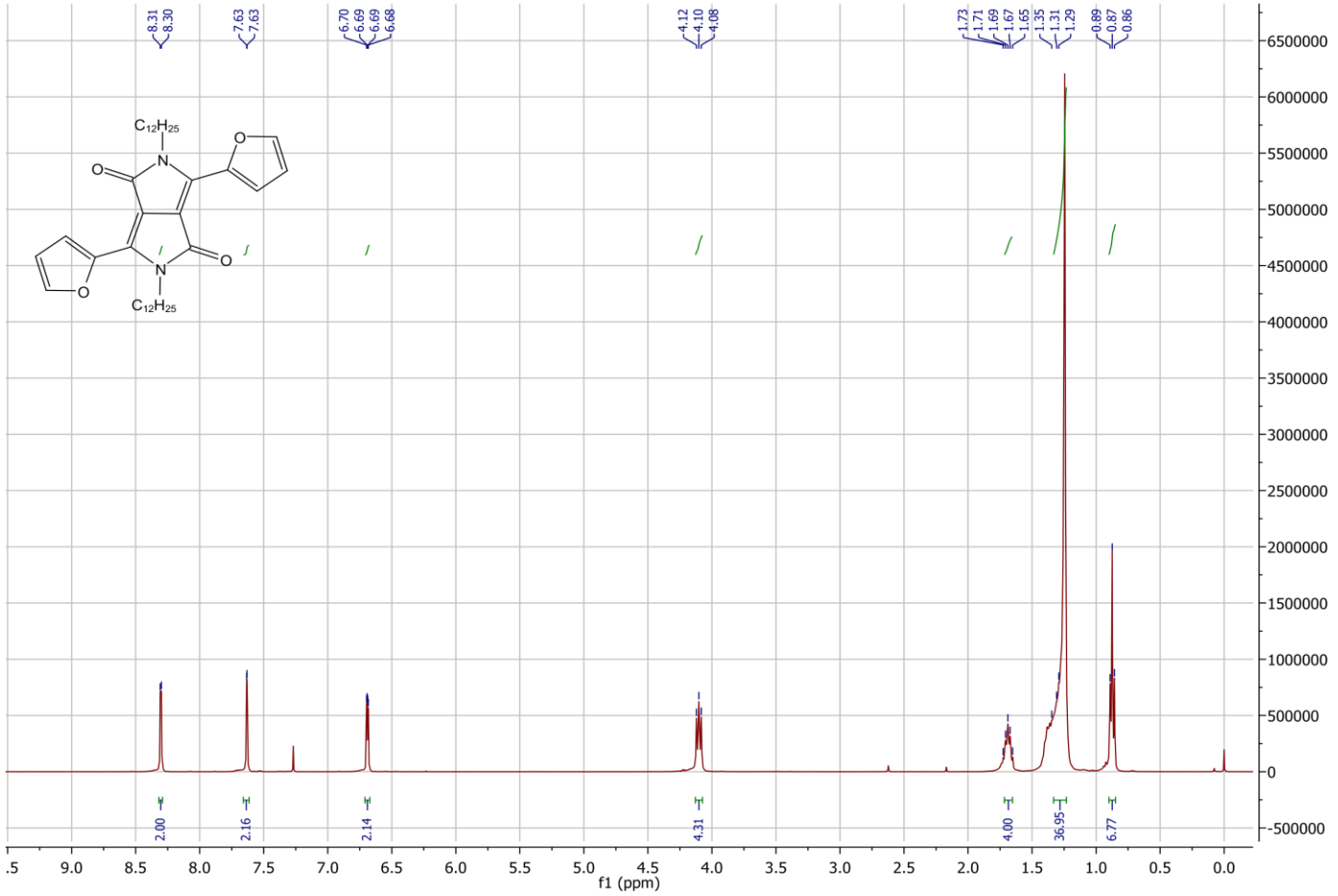

Figure A.7. [1]H-NMR spectrum of 2,5-didodecyl-3,6-di(furan-2-yl)-2,5-dihydropyrrolo[3,4-*c*]pyrrole-1,4-dione

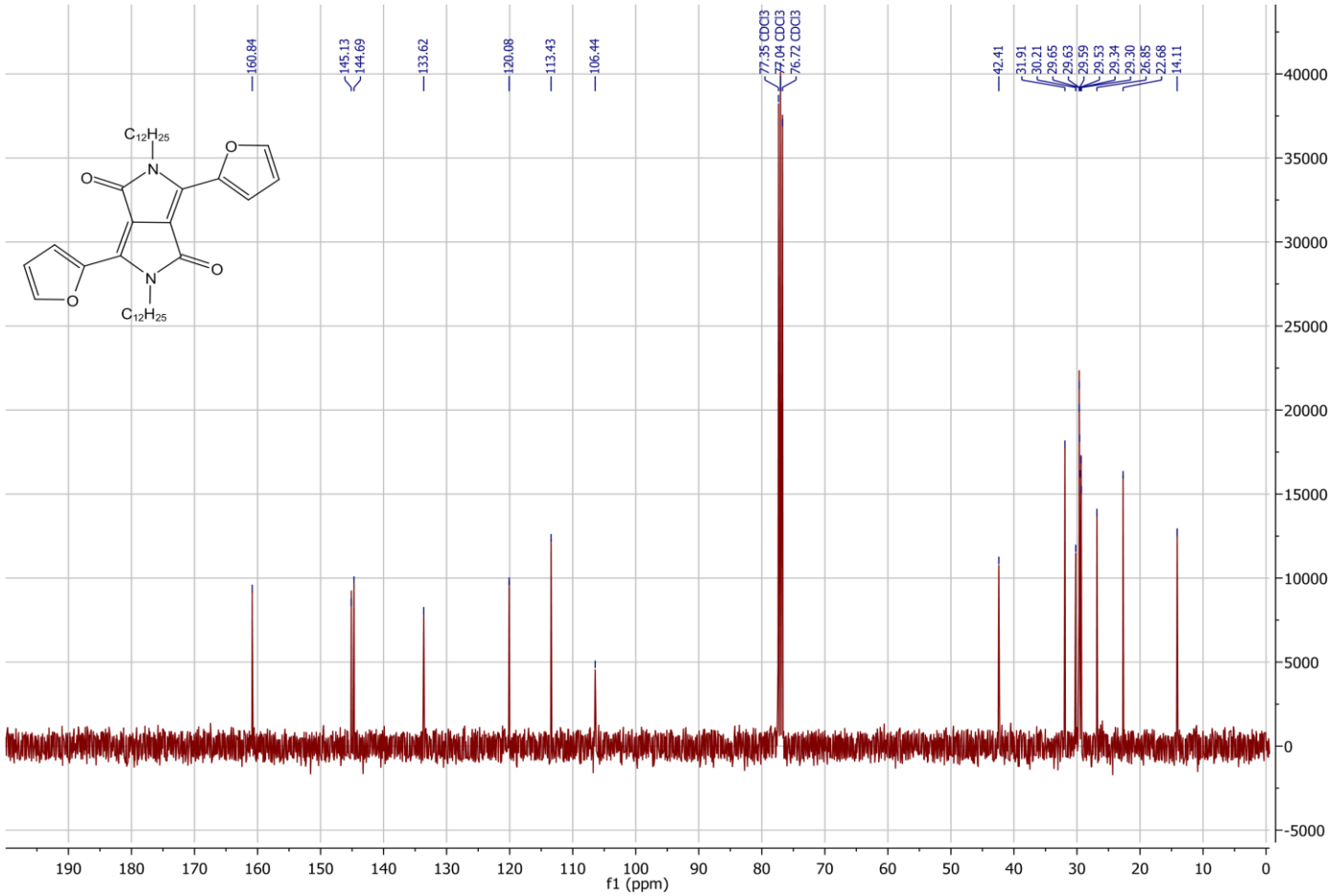

Figure A.8. ^{13}C-NMR spectrum of 2,5-didodecyl-3,6-di(furan-2-yl)-2,5-dihydropyrrolo[3,4-*c*]pyrrole -1,4-dione

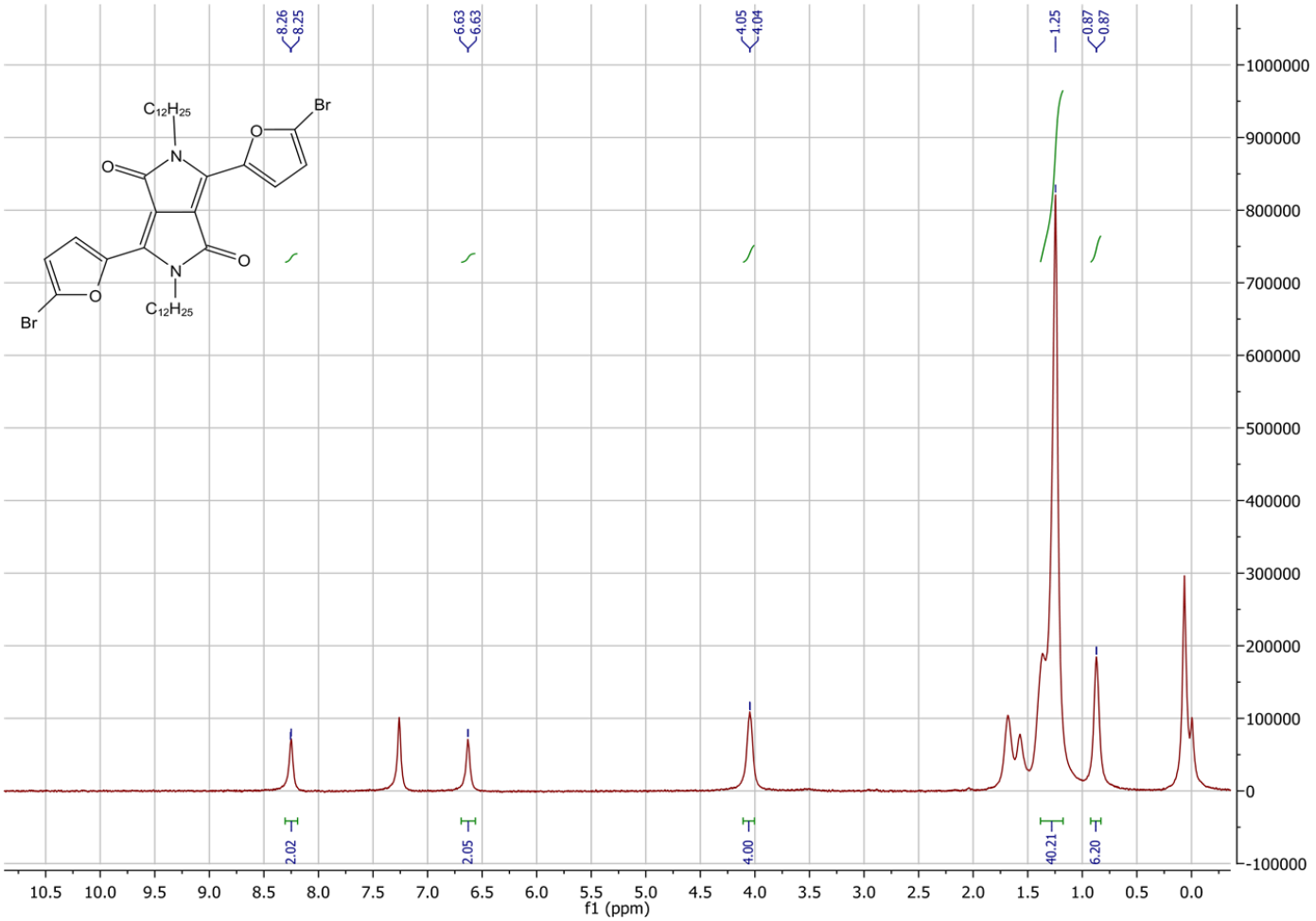

Figure A.9. [1]H-NMR spectrum of 3,6-bis(5-bromofuran-2-yl)-2,5-didodesil-2,5-dihydropyrrolo[3,4-*c*] pyrrol-1,4-dione

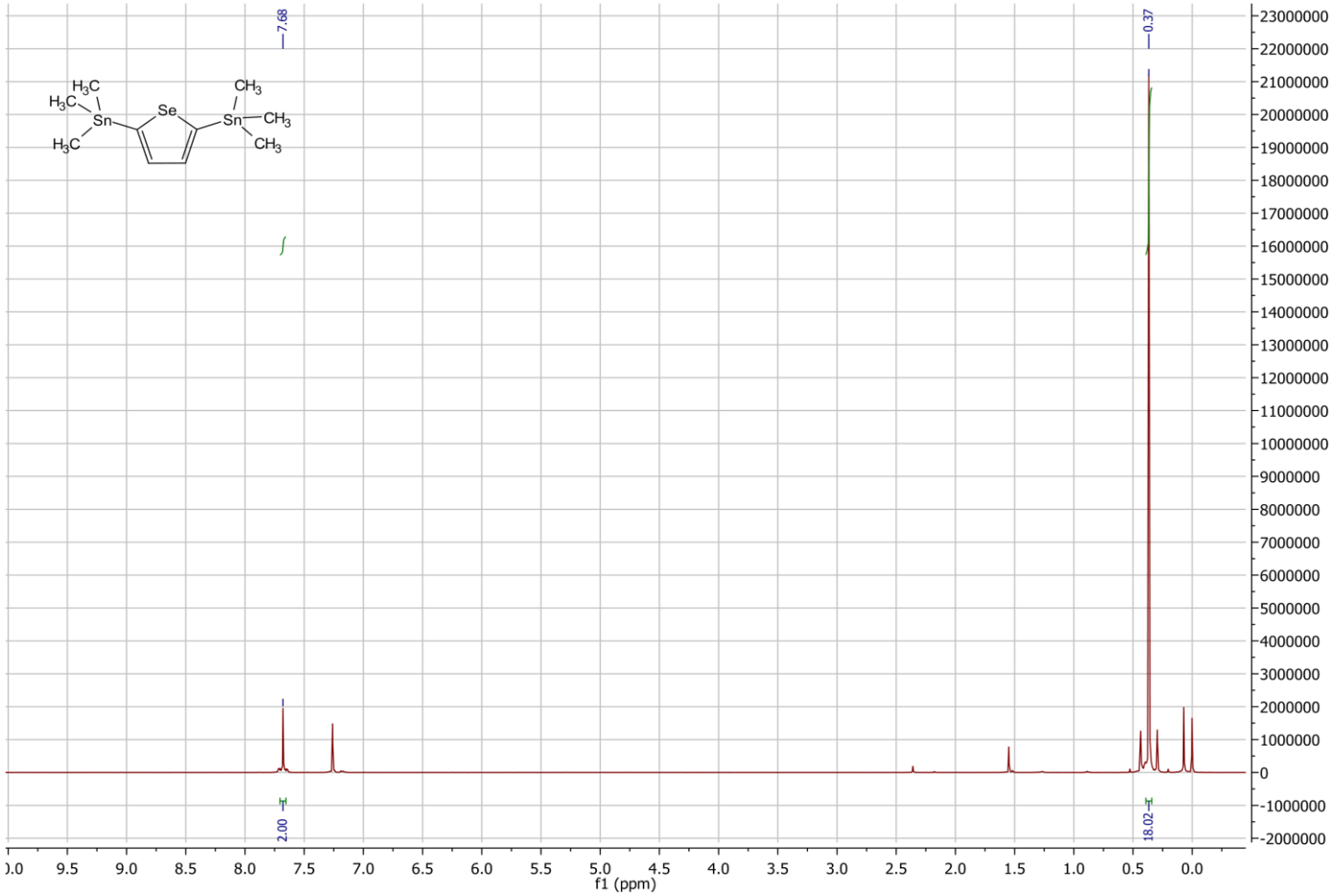

Figure A.10. [1]H-NMR spectrum of 2,5-bis(trimethylstannyl)-selenophene

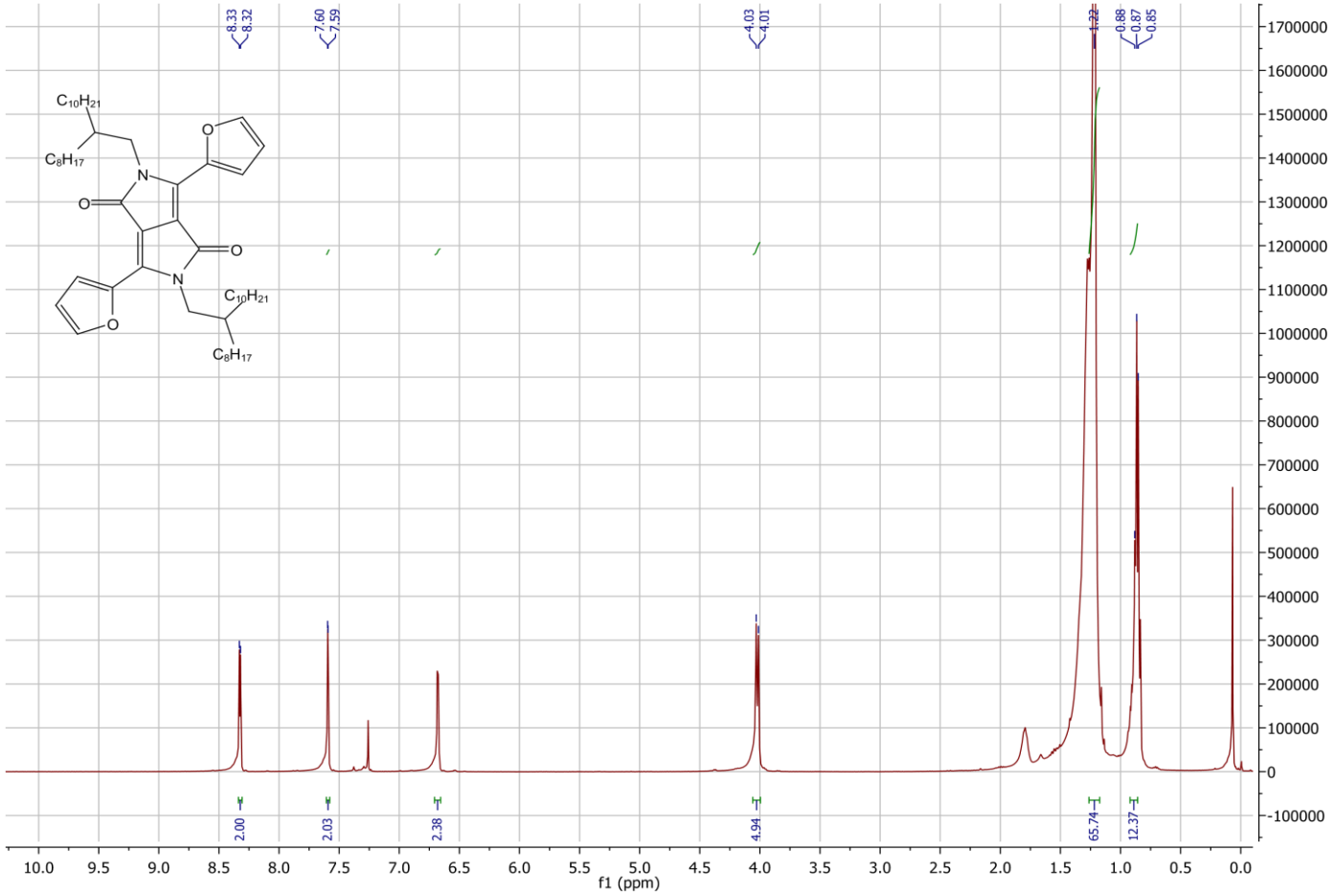

Figure A.11. ^{1}H-NMR spectrum of 3,6-di(furan-2-yl)-2,5-bis(2-octyldodecyl)-2,5-dihydropyrrolo[3,4-*c*] pyrrole-1,4-dione

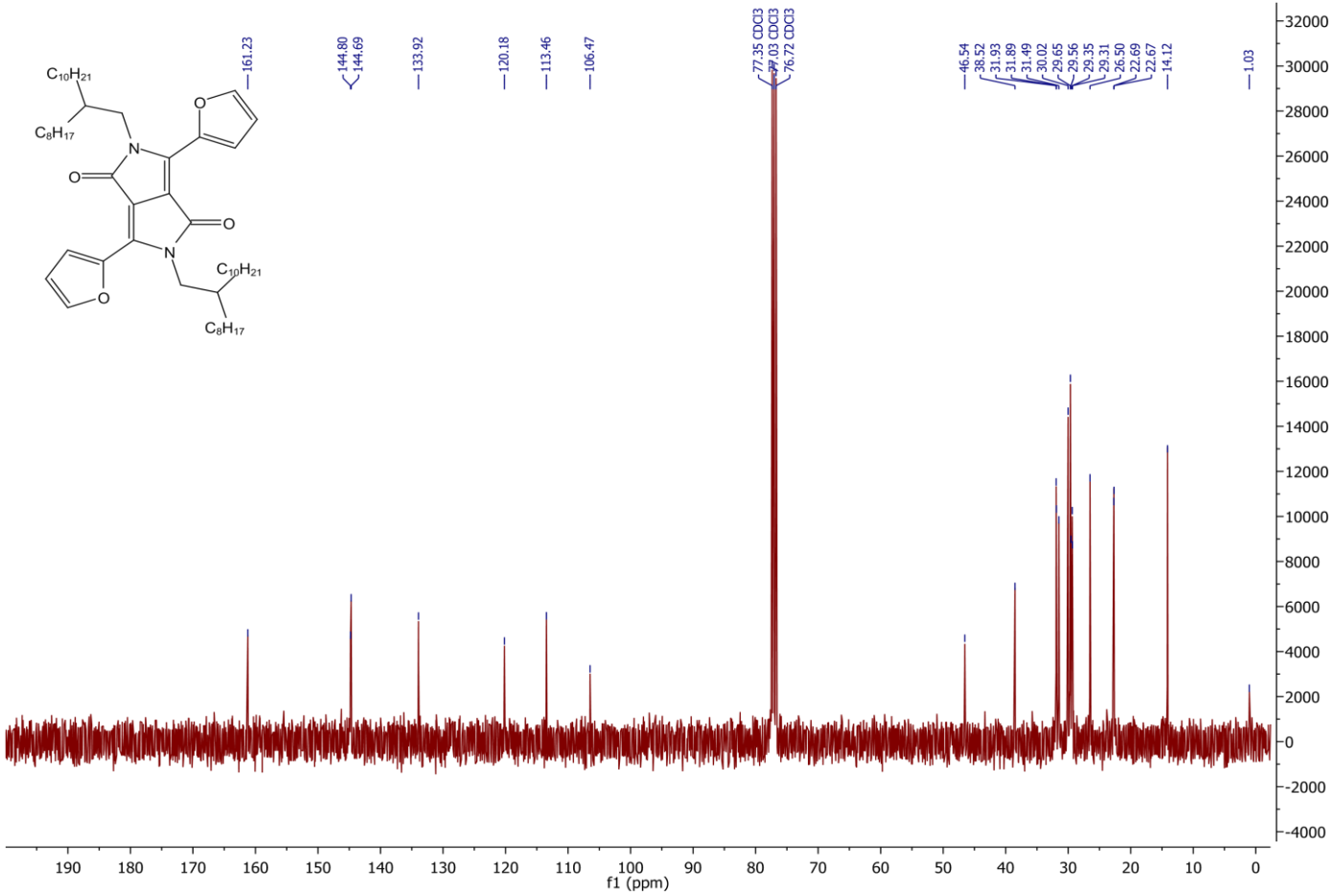

Figure A.12. ^{13}C-NMR spectrum of 3,6-di(furan-2-yl)-2,5-bis(2-octyldodecyl)-2,5-dihydropyrrolo[3,4-*c*] pyrrole-1,4-dione

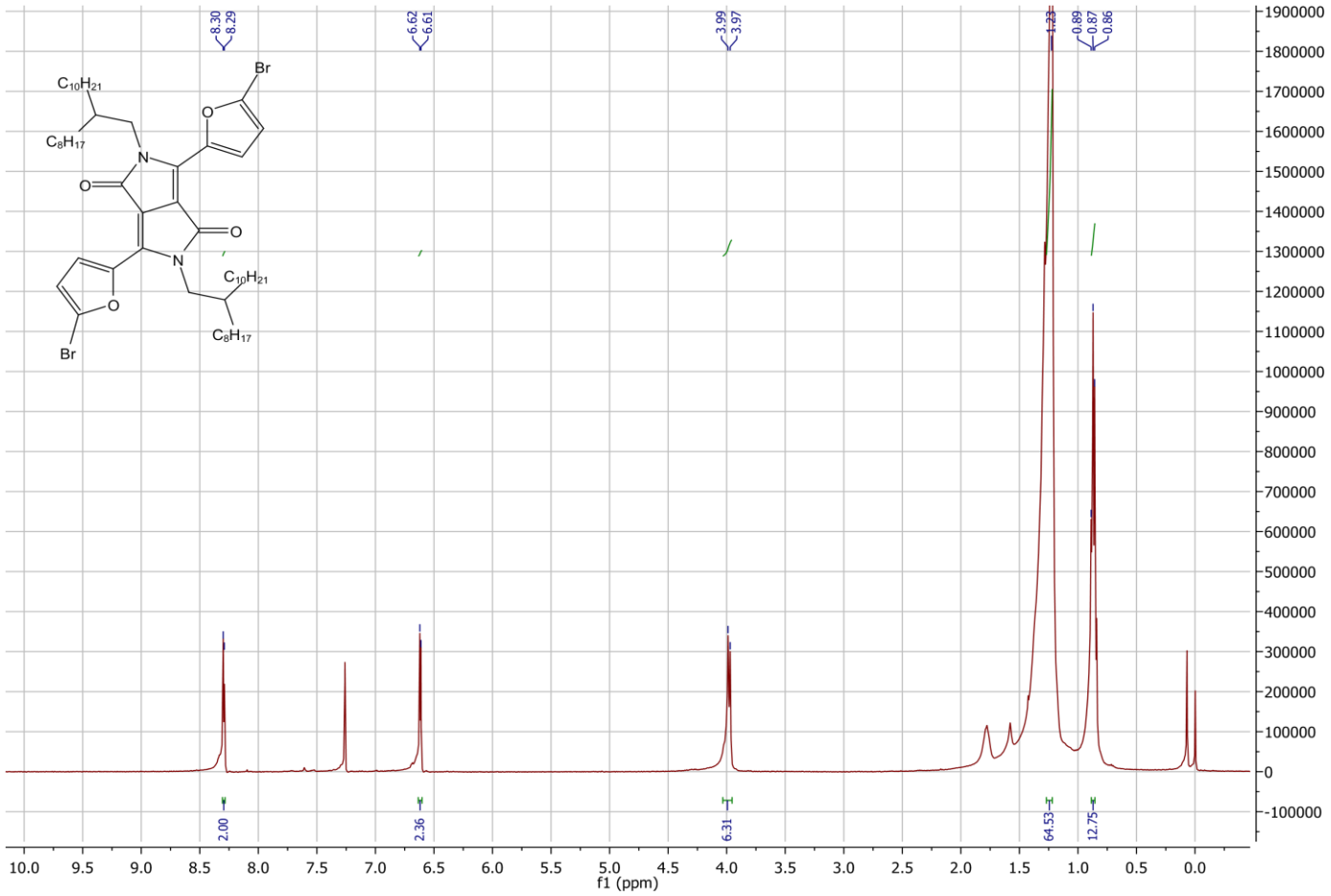

Figure A.13. ^{1}H-NMR spectrum of 3,6-bis(5-bromofuran-2-yl)-2,5-bis(2-octyldodecyl)-2,5-dihydropyrrolo [3,4-*c*]pyrrole-1,4-dione

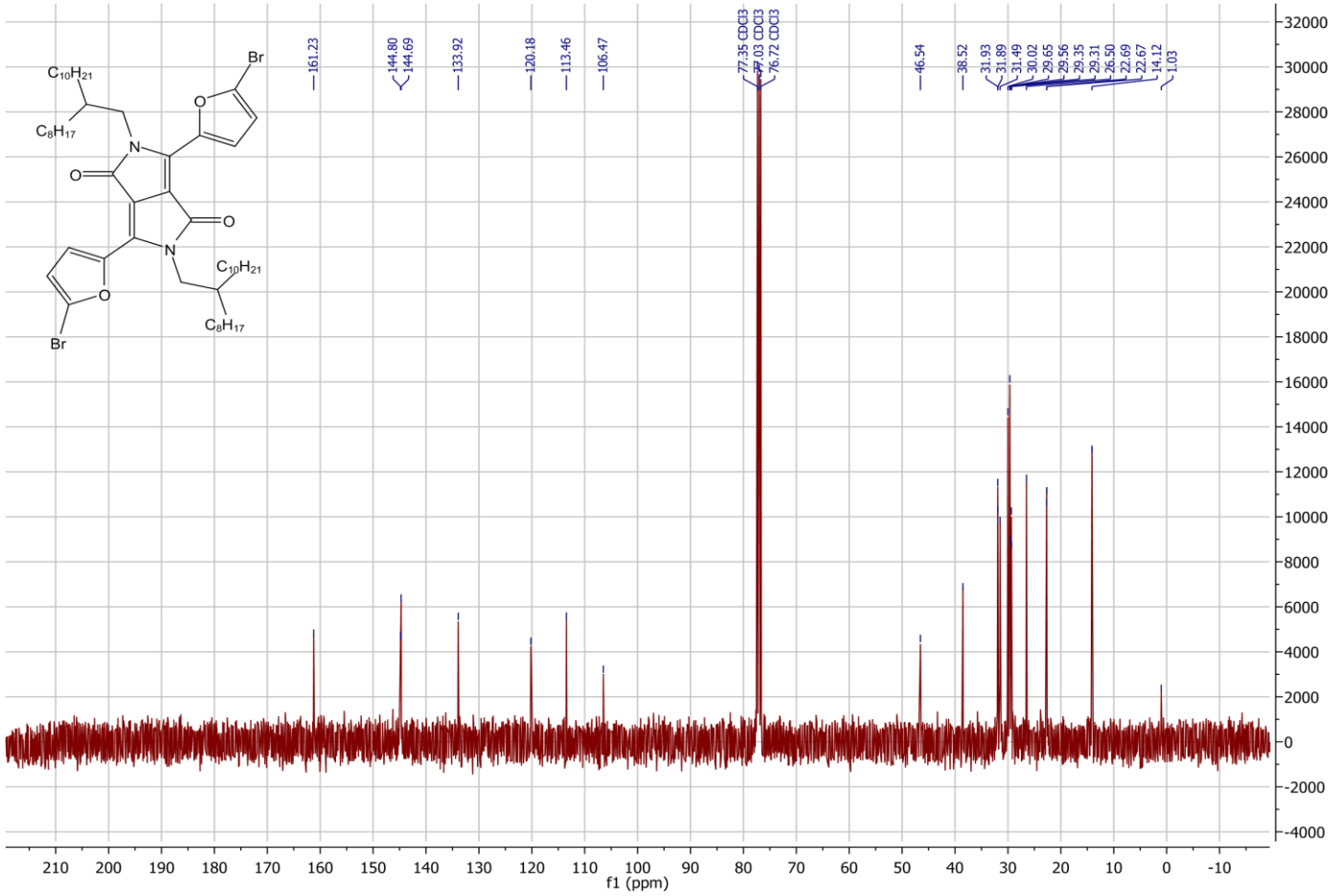

Figure A.14. ^{13}C-NMR spectrum of 3,6-bis(5-bromofuran-2-yl)-2,5-bis(2-octyldodecyl)-2,5-dihydropyrrolo [3,4-*c*]pyrrole-1,4-dione

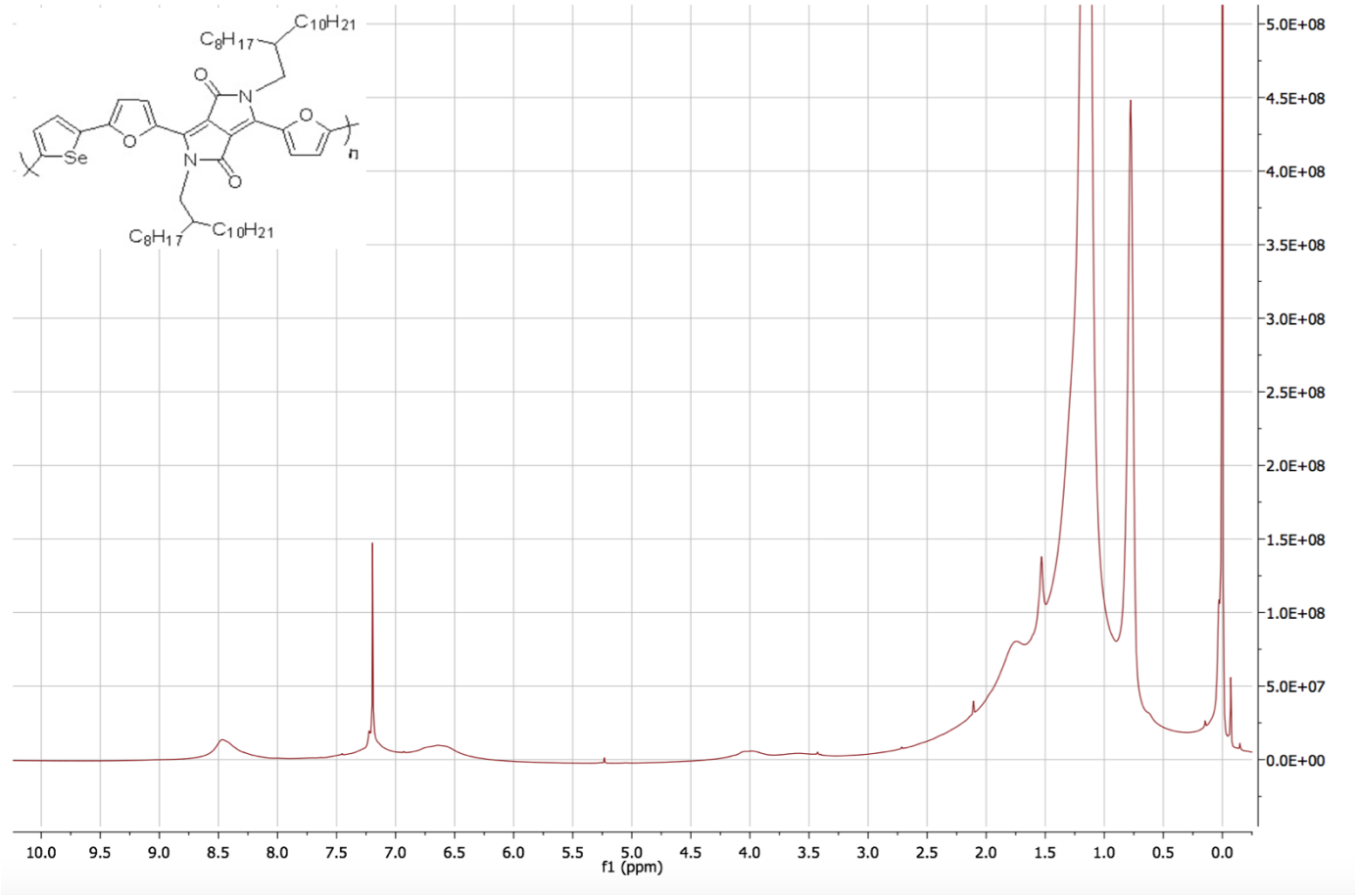

Figure A.15. [1]H-NMR spectrum of 3-(5-methylfuran-2-yl)-6-(5-(5-methylselenophen-2-yl)furan-2-yl)-2,5-bis(2-octyldodecyl)-2,5-dihydropyrrolo[3,4-*c*]pyrrole-1,4-dione **(P2)**

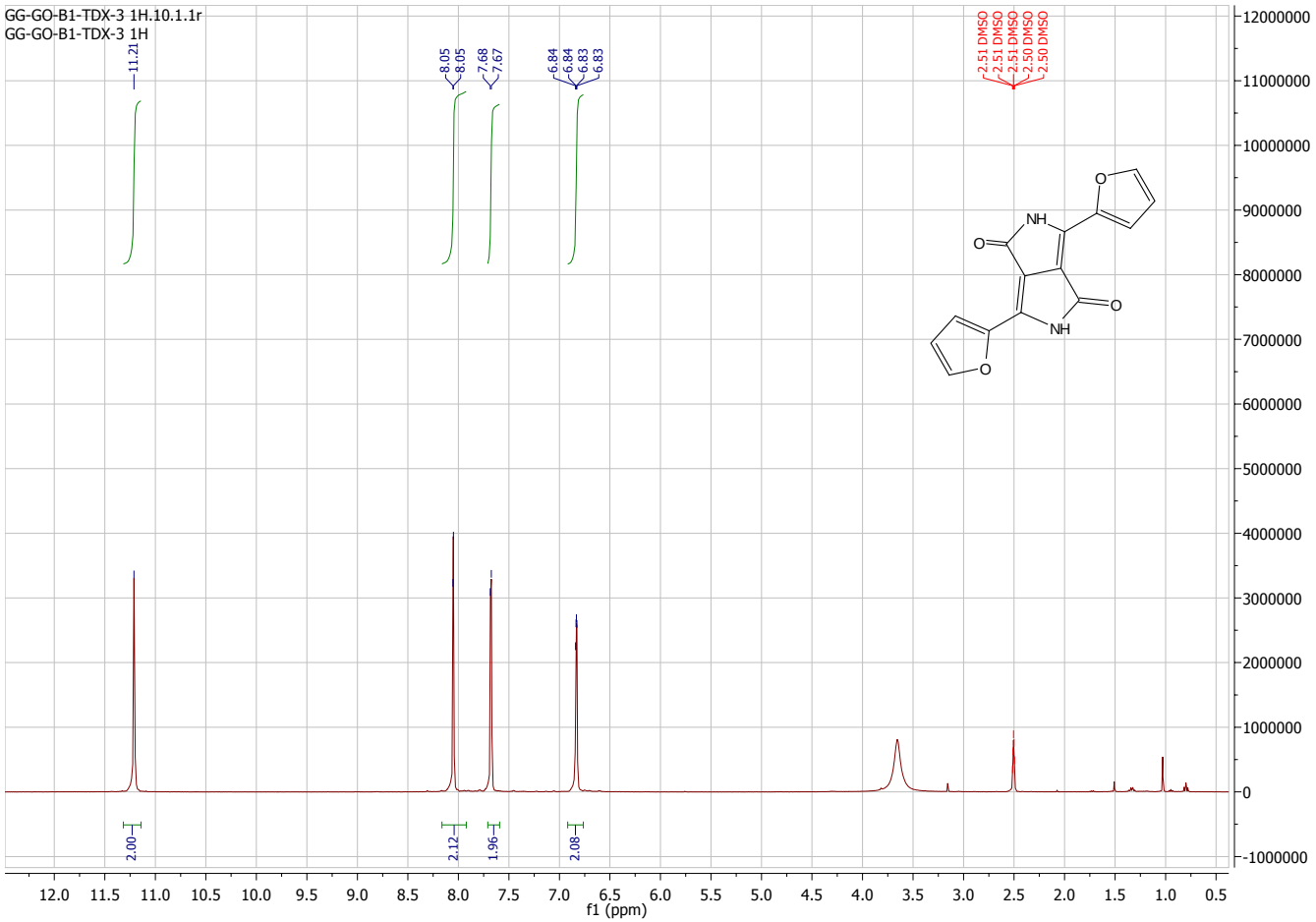

Figure A.16. ^{1}H-NMR spectrum of 3,6-di(furan-2-yl)-2,5-dihydropyrrolo[3,4-*c*]pyrrole-1,4-dione

Figure A.17. ^{13}C-NMR spectrum of 3,6-di(furan-2-yl)-2,5-dihydropyrrolo[3,4-*c*]pyrrole-1,4-dione

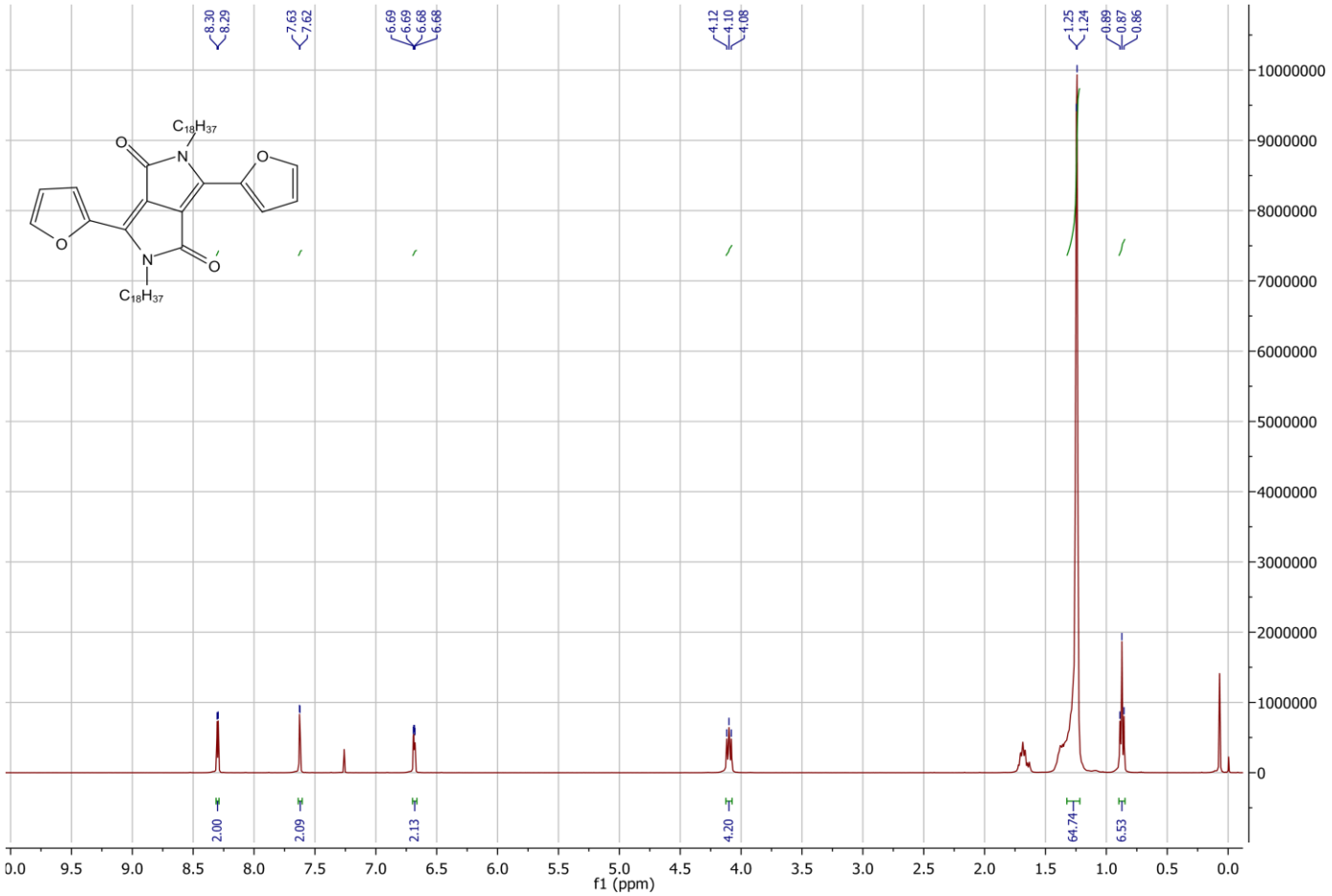

Figure A.18. [1]H-NMR spectrum of 3,6-di(furan-2-yl)-2,5-dioctadecyl-2,5- dihydropyrrolo[3,4-*c*]pyrrole-1,4-dione

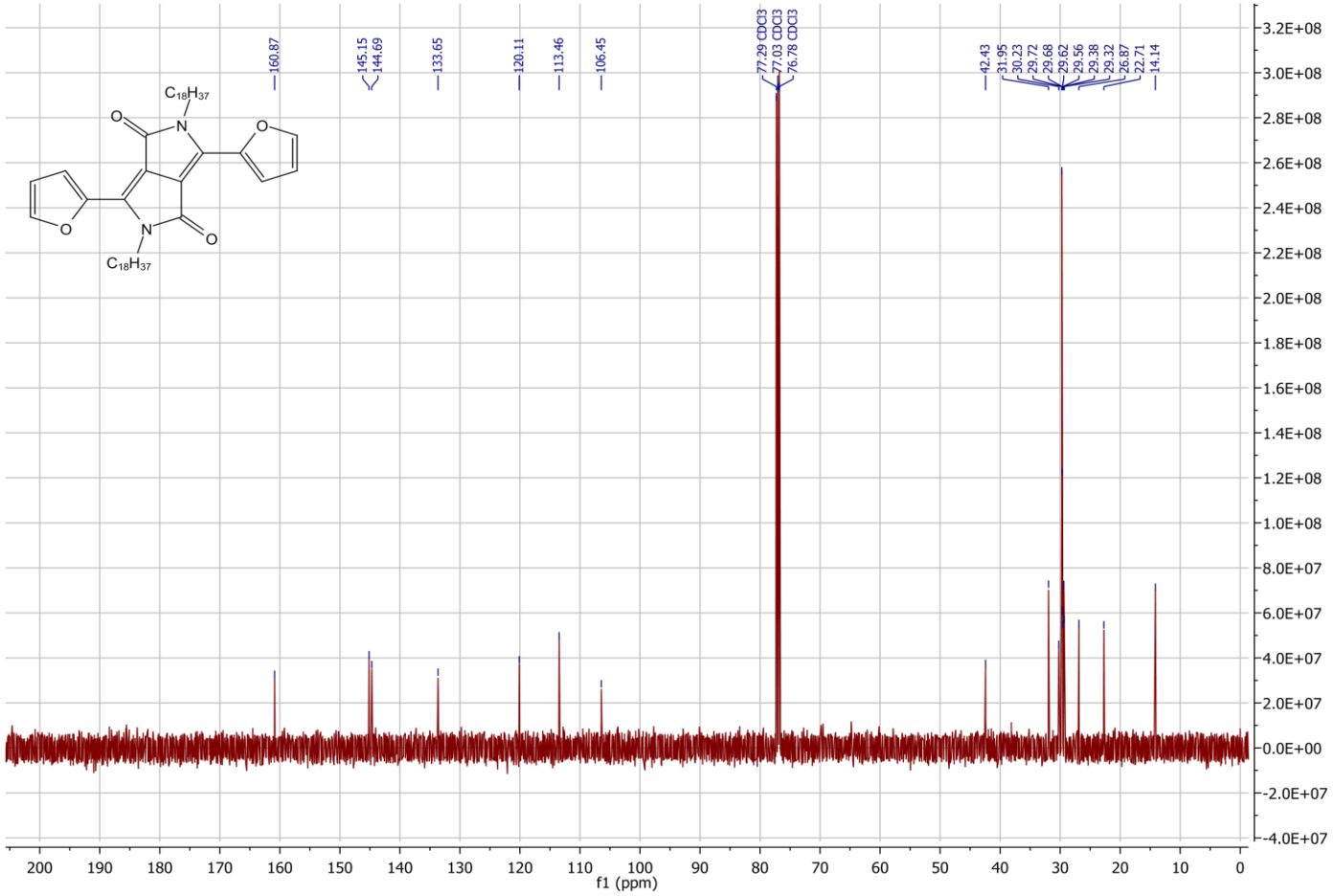

Figure A.19. ^{13}C-NMR spectrum of 3,6-di(furan-2-yl)-2,5-dioctadecyl-2,5- dihydropyrrolo[3,4-*c*]pyrrole-1,4-dione

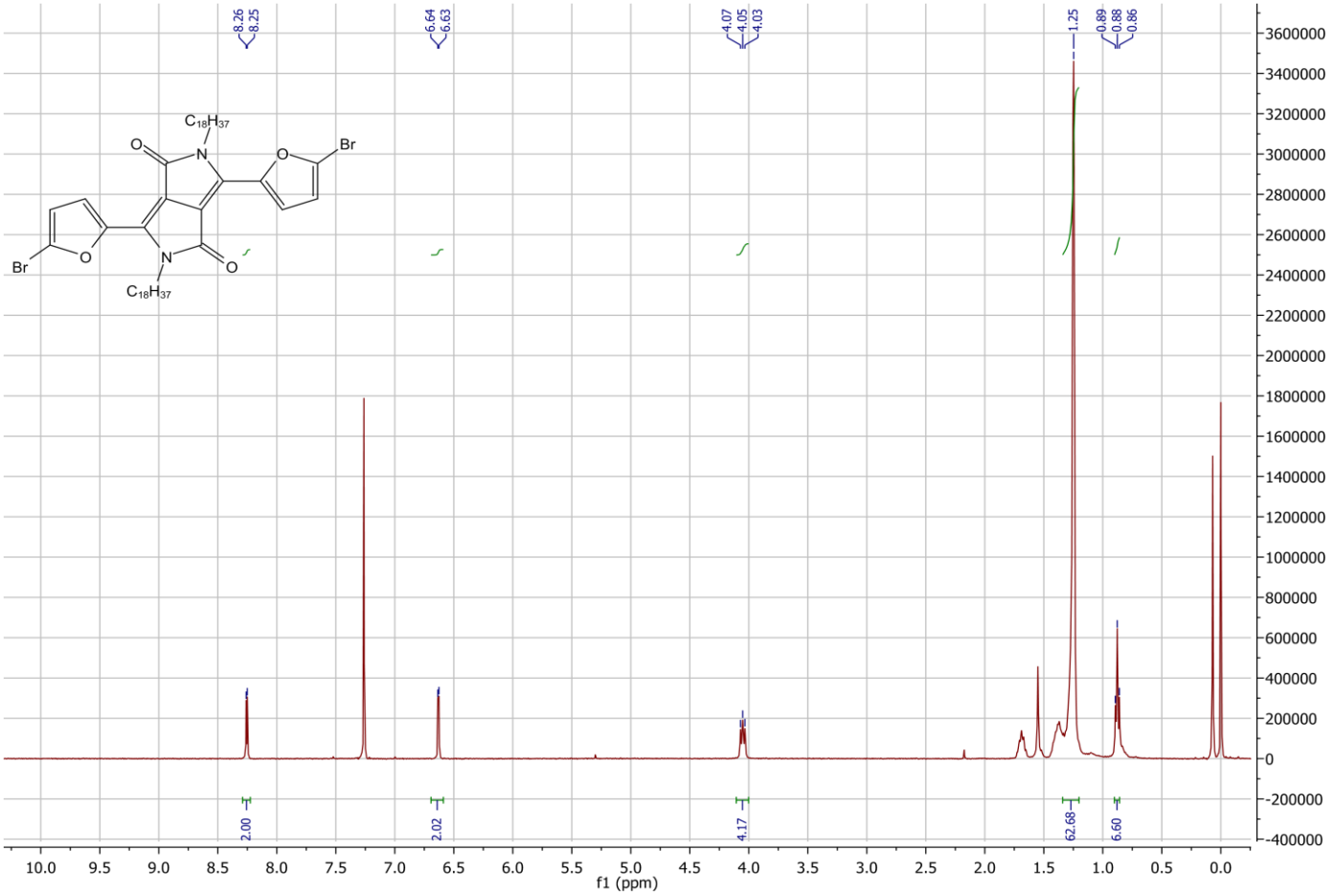

Figure A.20. [1]H-NMR spectrum of of 3,6-bis(5-bromofuran-2-yl)-2,5-dioctadecyl-2,5-dihydropyrrolo[3,4-*c*] pyrrole-1,4-dione

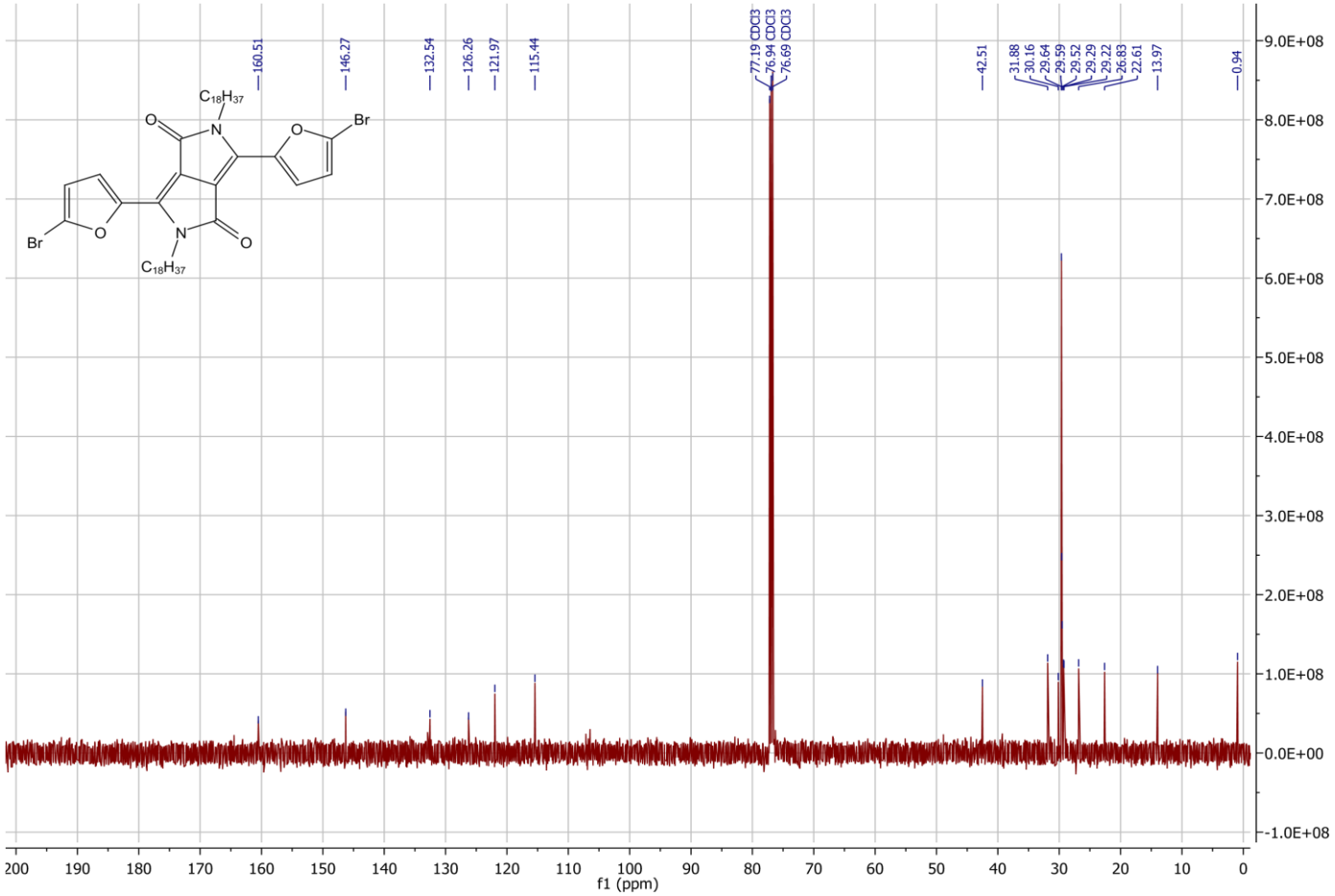

Figure A.21. ^{13}C-NMR spectrum of 3,6-bis(5-bromofuran-2-yl)-2,5-dioctadecyl-2,5-dihydropyrrolo[3,4-*c*] pyrrole-1,4-dione

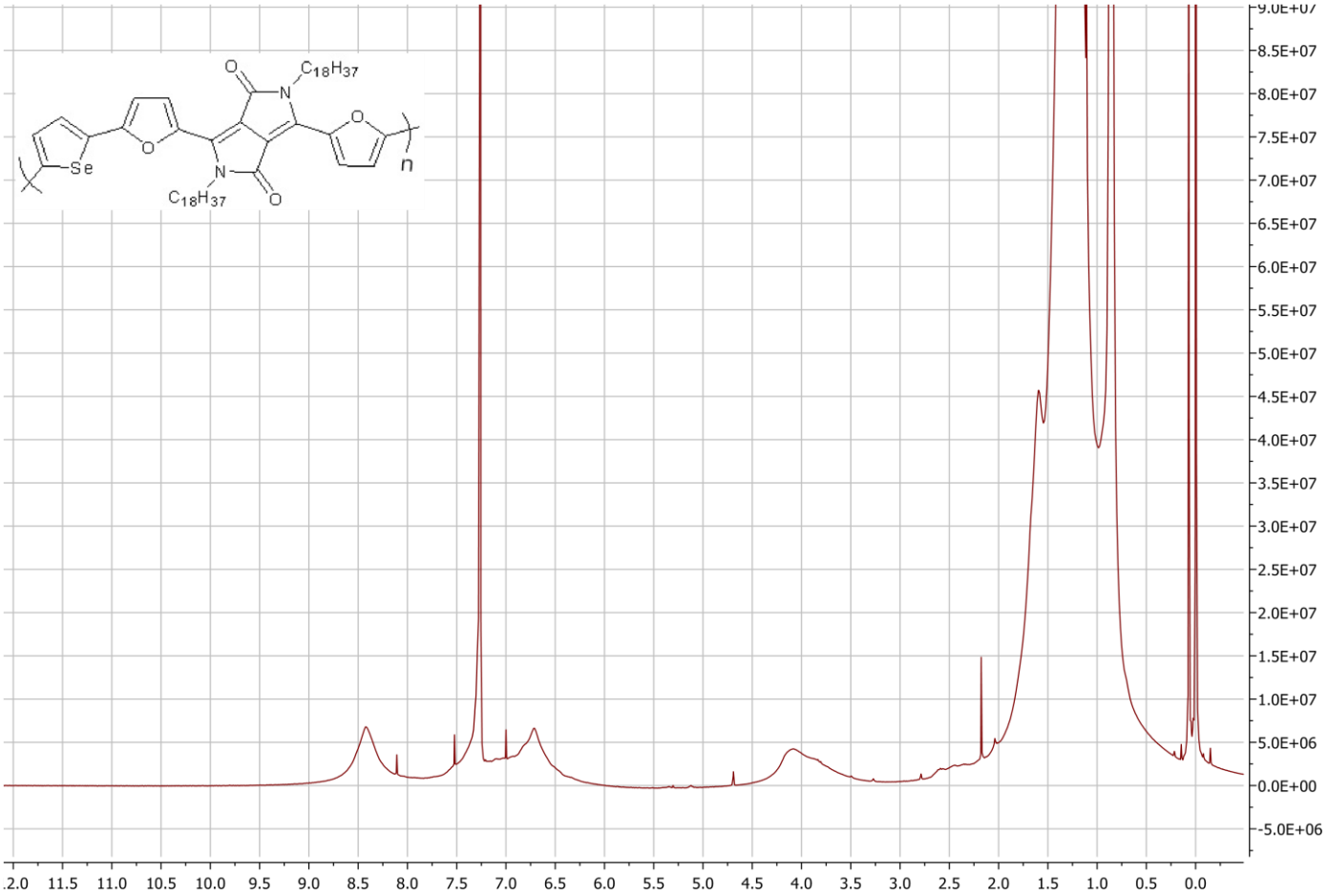

Figure A.22. ^{1}H-NMR spectrum of 3-(5-methylfuran-2-yl)-6-(5-(5-methylselenophen-2-yl)furan-2-yl) -2,5-dioctadecyl-2,5-dihydropyrrolo[3,4-c]pyrrole-1,4-dione **(P3)**